ANALYSIS OF THE DYNAMIC RESPONSES OF THE NORTHERN GUAM LENS AQUIFER TO SEA LEVEL CHANGE AND RECHARGE

H. Victor Wuerch
Benny C. Cruz
Arne E. Olsen

WERI

WATER AND ENVIRONMENTAL RESEARCH INSTITUTE OF THE WESTERN PACIFIC UNIVERSITY OF GUAM

Analysis of the Dynamic Response of the Northern Guam Lens Aquifer to Sea Level Change and Recharge

by

H. Victor Wuerch
Benny C. Cruz

Guam Environmental Protection Agency

&

Arne E. Olsen

Water & Environmental Research Institute
of the Western Pacific

University of Guam

Technical Report No. 118
November, 2007

ABSTRACT

Northern Guam Lens (Lens) is the primary fresh water resource on Guam. A plethora of research has been conducted upon the Lens; generally, this research has focused on aquifer processes that occur at a monthly or annual time scale. The focus of this paper is analysis of data that was collected, in a collaborative effort between the Guam Environmental Protection Agency, the United States Geological Survey, and the Water and Environmental Research Institute of the Western Pacific at the University of Guam, between May 25, 2004 and February 20, 2005, at a finer time-scale. This paper will demonstrate how climatic stimuli affect the water table and salt – fresh water interface differently depending on the time-scales considered. Presented herein, are time series of measurements that describe the upper and lower Lens boundaries, climatic variables, and an analysis of the cumulative effects of these variables on lens geometry. The results of the study clearly show that temporal variability in climatic conditions affected the distribution of both fresh water and salt water within the Lens. Large rapid fluctuations in the water table result from the onset and cessation of large rain events; whereas, more moderate rainfall result in a gradual rise of the water table during the early portion of the wet season. To the greatest extent the salt – fresh water interface was depressed during the study period. This was the result of the combined affects of a water table elevation fluctuation and sea level elevation decline. Large, short-term storm events tend to influence the upper portion of the salt – fresh water interface. Longer-term changes in the water table and sea level elevation influenced the entire salt – fresh water interface.

ACKNOWLEDGMENTS

TABLE OF CONTENTS

TABLE OF FIGURES

LIST OF TABLES

INTRODUCTION

Guam is the largest and most southern of the Mariana Islands, it is located at latitude 13°28' N., longitude 144°45' E (Figure 1, insert). Guam is approximately 48 km long and ranges from 18.5 to 6.4 km wide, with a total area of 550 km^2 (Figure 1). For hydrological purposes the island is divided into two regions of almost equal size (Figure 1) (Ward et al., 1965; Mink, 1976; and Mink and Vacher, 1997). The Pago-Adulop Fault separates the southern volcanic highland from the northern limestone plateau (Figure 2) (Mink, 1976; Mink and Vacher, 1997). The southern region is composed of deeply dissected upland underlain primarily by volcanic rock. This region of the island is characterized by a proliferation of streams; several of these streams have been developed as surface water resources (Ward et al., 1965). Due to the low permeability of the volcanic rock in the southern region little groundwater development has occurred (Ward et al, 1965; Mink, 1976). Northern Guam is composed of an undulating limestone plateau (Figure 2) (Ward et al., 1965; Mink, 1976; and Mink and Vacher, 1997). This region is characterized by very permeable eogenetic, karst limestone (Mylorie et al., 2001). A fresh water lens, which partially floats on salt water, has developed within the limestone plateau of northern Guam (Ward et al., 1965; Mink, 1976; and Mink and Vacher, 1997).

The Northern Guam Lens (Lens) is the primary fresh water resource on Guam. The Lens currently provides approximately 2,000 l s^{-1} (40 million gallons per day) to the Guam Water Authority, United States Navy, United States Air Force, and several private water producers (Contractor and Jensen, 2000; Jocson et al., 2002). Several studies have been conducted to determine the sustainable yield of the lens. Sustainable yield has been defined as the rate at which water can be extracted from the lens without impairing water quality through increased chloride concentrations from salt water intrusion. The sustainable yield of the Lens has been estimated at between 2,500 l s^{-1} (50 mgd) (Mink, 1976; CDM, 1982) and 3,000 l s^{-1} (60 mgd) (BCG, 1992). Although the cumulative production rate for the entire lens is less than current estimates of sustainable yield localized salt water intrusion has occurred (McDonald and Jenson, 2003). The degradation of water quality at individual wells or in well fields has been attributed to inappropriate well construction and over production at individual wells or well fields (McDonald and Jenson, 2003).

A plethora of research has been conducted on the Lens (Mink, 1976; Contractor and Srivastava, 1990; Contractor and Jensen, 2000; Jocson et al., 2002); generally, this research has focused on aquifer processes that occur at a monthly or annual time scale (Contractor and Srivastava, 1990; Contractor and Jensen, 2000). The focus of this paper is analysis of data that was collected, in a collaborative effort between the Guam Environmental Protection Agency, the United States Geological Survey, and the Water and Environmental Research Institute of the Western Pacific at the University of Guam, between May 25, 2004 and February 20, 2005, at a finer time-scale. This paper will demonstrate how climatic stimuli affect the water table and salt – fresh water interface differently depending on the time-scales considered. Presented herein, are time series of measurements that describe the upper and lower Lens boundaries, climatic variables, and an analysis of the cumulative effects of these variables on lens geometry.

Figure 1. General geology map of Guam, illustrating the relative positions of limestone (north, and south eastern coast) and volcanic rock (the interior south). Additionally, the general location of the Pago-Adulop fault is shown. The map inclusion illustrates the location of Guam within the tropical north western-Pacific
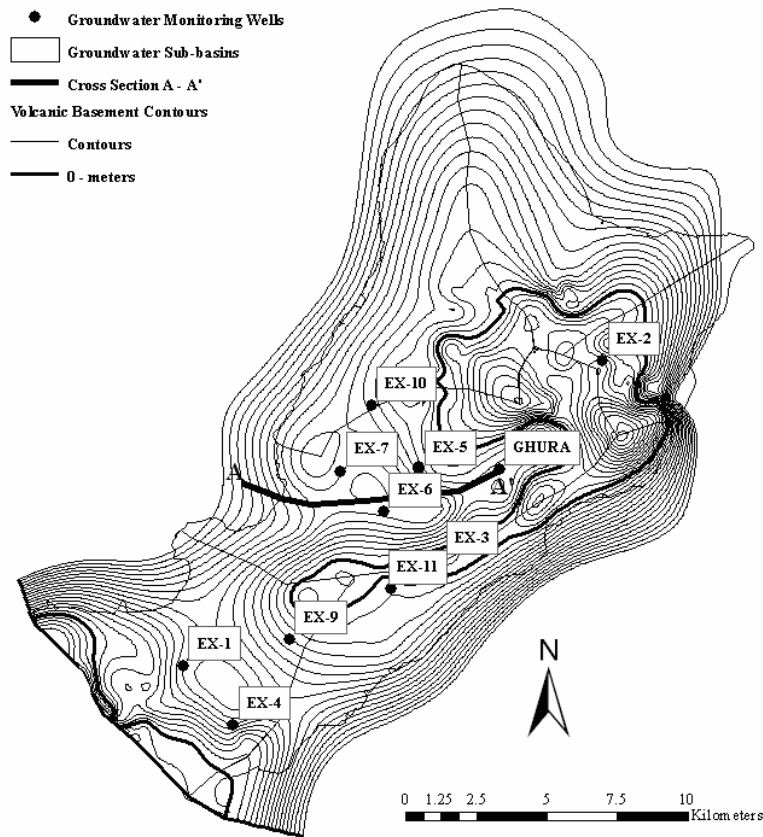
Figure 2. Map of the Northern Guam Lens, including the location of groundwater monitoring wells, groundwater sub-basins and the elevation contours of the volcanic basement rock. Cross-section A-A' is illustrated in Figure 3.

Conceptual Model

The best conceptual model for karst carbonate islands is the so-called Carbonate Island Karst Model (CIKM) (Keel et al., 2004). This model classifies carbonate islands based upon their geologic and hydrogeologic characteristics. Also important to the CIKM are how these characteristics have changed over time due to enhanced dissolution, relative sea level change, relative island size change, and effects of eogenetic environment on young limestone (Mylroie et al., 2001). The model classifies islands as one of four types, or mixtures of the four types, depending on the complexity of the freshwater lens, carbonate geology, and non-carbonate geology (Mylroie et al., 1999). The first island type, the simple carbonate island, is characterized by a fresh water lens that floats on salt water within a carbonate aquifer. The lens, within a simple carbonate island, does not interact with non-carbonate rock. The second island type, the carbonate cover island is characterized by a fresh water lens that intersects non-carbonate rocks that are not sub-aerially exposed. The third island type, the composite island is characterized by non-carbonate rock exposed at the ground surface. The fourth island type, the complex island, is characterized by a carbonate aquifer that interacts with the non-carbonate rock in a complex way due to tectonic modification of the aquifer (Keel et al., 2004). The limestone plateau of Northern Guam displays characteristics of simple, carbonate cover, and composite island types (Mylroie et al., 2001).

The karst structures that have developed within the northern plateau of Guam have a significant influence upon its hydrogeologic characteristics (Mylroie et al., 2001). Precipitation incident upon the northern plateau of Guam may follow one of many pathways or be transferred between different pathways. In the first pathway water percolates into the soil where it is either absorbed by plant roots and transmitted back to the atmosphere or it continues to the limestone, vadose zone. The second potential pathway is for water to bypass the soil and percolate directly into the limestone, vadose-zone through dissolution features (i.e. sink holes, banana holes). Once into the limestone, vadose-zone recharge water may percolate through the primary porosity of the limestone as diffuse flow or through the secondary, dissolution enhanced, porosity as discrete flow. At this point water may transfer from the primary porosity to the secondary porosity or visa-a-versa, depending upon on the local, hydraulic-potential field. Regardless of the pathway that percolating water takes though the limestone-vadose zone, the vast majority will eventually arrive at the phreatic surface. Once in the Lens water may flow through secondary or primary porosity. Studies of well hydraulics have shown a variation in hydraulic conductivity of several orders of magnitude (60 (Mink, 1976) to 6,300 $m\ d^{-1}$ (Ayers and Clayshulte, 1984)) and a large range in aquifer porosity (1.5 to 26 %) (Ayers and Clayshulte, 1984). The wide range in aquifer properties is characteristic of eogenetic, karst, limestone-aquifers. Darcian groundwater flow models of the Lens generally have used hydraulic conductivities and porosities at the upper end of the measured range (6100 $m\ d^{-1}$ and 20 %) to provide adequate history matching (Jocson, et al., 1999). This indicates that a large proportion of the total aquifer flow occurs through the largest pores.

Mathematical Model

The study of the interaction of fresh water and salt water, in costal or island environments, began during the last half of the nineteenth century and the beginning of the twentieth century. Two researchers Ghyben and Hertzberg published equations that explained the steady state behavior of a fresh water lens based upon the assumption of static fresh and salt water and that there was an abrupt transition between the salt water and fresh water (Cooper, 1964). By making these assumptions Ghyben and Hertzberg were able to apply Archimedes principle, which states the volume of a fluid that is displaced by placing a body into that fluid is proportional to the relative density differences of the body and the fluid. Therefore, by examining a unit area, the depth below sea level z [L] to a point on the interface is:

$$z = \frac{\rho_f}{\rho_s - \rho_f} h \ ,$$
1)

where ρ_f [ML^{-3}] is the density of fresh water, ρ_s [ML^{-3}] is the density of salt water, and h [L] is the hydraulic head of fresh water at the point on the interface. Generally, the density of fresh water is taken to be approximately 1000 kg m^{-3} and the density of salt water is taken to be approximately 1025 kg m^{-3}; therefore, the density excess is 40 [-] (Cooper, 1964). In homogenous, static, aquifers this results in the, all too common, simplifying assumption that the depth of the salt water interface is 40 times the freshwater hydraulic head.

The equations derived by Glover (1964) and Henry (1964) were simplified by Mink (1976) to determine the steady-state, hydraulic head within the Lens under differing pumping rates assuming a constant infiltration rate. Mink (1976) combined, the principle of continuity of mass, Darcy's Law, and the Ghyben – Hertzberg relationship (equation 1) and arrived at the relationship:

$$h^2 = h_o^2 - \frac{2xD}{41K}$$
2)

where h [L] is the steady-state, hydraulic head under a specified pumping condition, D [L^{3}T^{-1}L^{-2}] is the pumping rate per unit area, K [LT^{-1}] is the hydraulic conductivity, h_o [L] is the steady-state, hydraulic head prior to pumping, x [L] is the width of the aquifer, and the constant 41 was related to the density excess. Mink used this relationship to estimate the sustainable yield of the Lens (Mink, 1976). Mink later (BCG, 1992) developed a transient solution that he used to determine the sustainable yield of the Lens under a simple harmonic infiltration regime.

Within the forgoing discussion all of the solutions presented simplified the salt water – fresh water aquifer system to arrive at analytical or quasi –analytical solutions. Specifically, all have considered a vertical two-dimensional aquifer cross section, where the fresh water floats upon a static salt water body. The interface of the salt and fresh water has been taken to be abrupt and mixing of salt and fresh water was not allowed. While maintaining the no mixing and abrupt interface condition, Contractor et al. (1981) developed a finite element solution, which allows for complex domain geometry,

temporally and spatially variable boundary conditions, and depth integrated salt water – fresh water flow. The second order partial differential equations derived for this finite element solution are:

Freshwater

$$\left(S^f + \frac{n\gamma^f}{\Delta\lambda}\right)\frac{\partial h^f}{\partial t} - \frac{n\gamma^s}{\Delta\gamma}\frac{\partial h^s}{\partial t}$$

$$= \frac{\partial}{\partial x_i}\left(K^f_{z_i,x_j}b^f\frac{\partial h^f}{\partial x_j}\right) + N + q^f_p - \frac{K^f}{b^f_o}\left(h^f - h^o\right)$$

3)

Saltwater

$$\frac{\partial}{\partial x_i}\left(K^s_{z_i,x_j}b^s\frac{\partial \phi^s}{\partial x_j}\right) + q^s_p = \left(S^s + \frac{n\gamma^s}{\Delta\gamma}\right)\frac{\partial \phi^s}{\partial t} - \frac{n\gamma^f}{\Delta\gamma}\frac{\partial \phi^f}{\partial t}$$

4)

where x_i [L] is the ith spatial direction (e.g., x, y, and z), K [LT^{-1}] is the hydraulic conductivity tensor, b [L] is the thickness, h [L] is the hydraulic head, N [L^{3}T^{-1}L^{-2}] is recharge, q [L^{3}T^{-1}L^{-1}] is fluid sources, n [-] is porosity, γ [ML^{-2}T^{-2}] is specific weight, S is the storativity [-] and t [T] is time. In both equations the superscripts f and s indicate fresh water and salt water, respectively (Contractor and Sirvastava, 1990). This finite element solution has been applied extensively to the Lens (Contractor, 1981a; Contractor, 1981b; Contractor et al., 1981; Contractor and Sirvastava, 1990; Contractor and Jensen, 2000; Jocson et al., 2002). Generally, it has been used to investigate the processes affecting the water table elevation. However, Contractor et al. (1981) found that the process that affect the water table also affect the interface; however, the interface response lagged behind the water table.

Cooper (1964) noticed that the salt – fresh water transition zone in the Biscayne Aquifer was not abrupt. This led him to conclude that salt water and fresh water within the transition zone were mixing due to diffusion and lateral and transverse, velocity-dependent dispersion (Figure 3). Cooper (1964) reasoned that salt water was diluted by mixing with the overlying fresh water. The diluted salt water was then forced upward due to density differences and was subsequently replaced by non-dilute salt water (Figure 2). In order to remove the no mixing assumption and provide a more complete description of the salt – fresh water aquifer system the advection-dispersion equation must be incorporated into the mathematical description and the water flow equation must be formulated to allow density dependent flow.

Voss and Provost (2002) presented a finite element solution to the three-dimensional, density-dependent, unsaturated, fluid-flow equation coupled with the advection-dispersion equation.
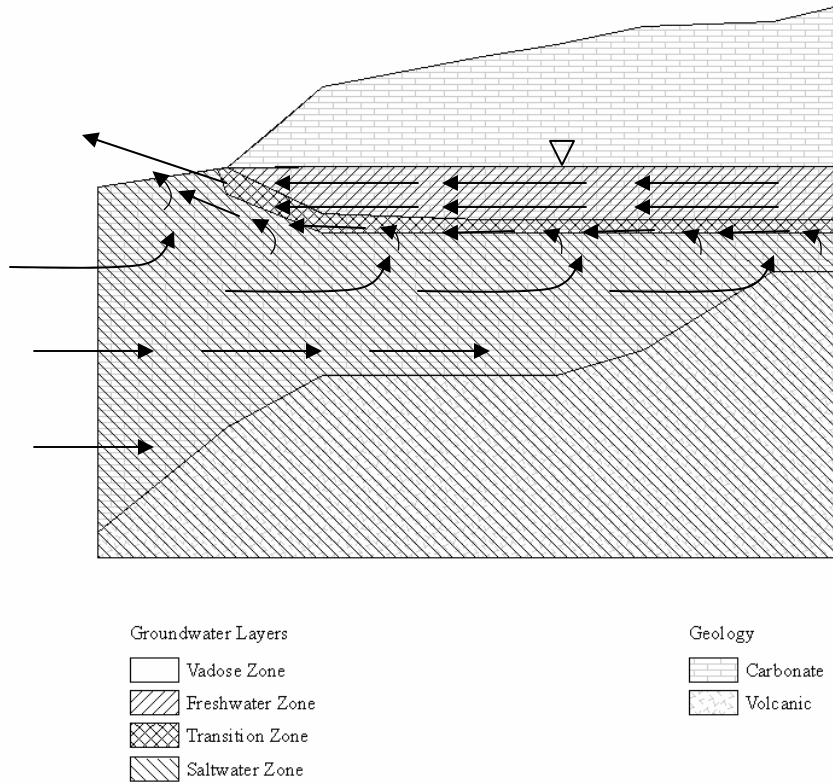
Figure 3. Schematic diagram of the Lens from A to A' on Figure 2. Arrows indicate the approximate direction of water flow. Approximate vertical exaggeration 1 to 15.

The fluid-flow equation is:

$$\left(S_w \rho S_{op} + \varepsilon \rho \frac{\partial S_w}{\partial p} \right) \frac{\partial p}{\partial t} + \left(\varepsilon S_w \frac{\partial p}{\partial C} \right) \frac{\partial C}{\partial t} =$$
$$\nabla \cdot \left[\left(\frac{\underline{\underline{k}} k_r \rho}{\mu} \right) \cdot \left(\nabla p - \rho g \right) \right] + Q_p$$

5)

where S_w [-] is the water saturation, ρ [ML^{-3}] is the density, S_{op} [LT^{2}M^{-1}] is the specific pressure storativity, ε [-] is the porosity, p[ML^{-1}T^{-1}] is the fluid pressure, C [M$_s$M^{-1}] is the solute mass fraction, k [L^2] is the permeability tensor, k_r [-] is the relative permeability, μ [ML^{-1}T^{-1}] is the viscosity, g [LT^{-2}] is the acceleration due to gravity and Q_p [ML^{-3}T^{-1}] is fluid sources and sinks (Voss and Provost, 2002). The first term of the left-hand-side (LHS) of equation 5 represented the time rate of change in fluid mass due to changes in water storage and desaturation of the aquifer. The second term on the LHS represented the time rate of change in fluid mass due to changes in the solute mass. The terms of the right-hand-side (RHS) of equation 5 represented advection of the fluid, following Darcy's law, and sources and sinks of fluid, respectively. The advection-dispersion equation is:

$$\frac{\partial(\varepsilon S_w \rho C)}{\partial t} + \frac{\partial\left[(1-\varepsilon)\rho_s C_s\right]}{\partial t} = -\underline{\nabla} \cdot \left(\varepsilon S_w \rho \underline{v} C \right)$$
$$+ \underline{\nabla} \cdot \left[\varepsilon S_w \rho \left(D_m \underline{\underline{I}} + \underline{\underline{D}} \right) \cdot \underline{\nabla} C \right] + \varepsilon S_w \rho \Gamma_w + (1-\varepsilon)\rho \Gamma_s + Q_p C^*$$

6)

where v [LT^{-1}] is fluid velocity, D_m [L^{2}T^{-1}] is molecular diffusion, I [-] is the identity tensor, D [L^{2}T^{-1}] is the dispersion tensor, Γ_w and Γ_s [M$_s$M^{-1}T^{-1}] are the solute sources due to production within the fluid and solid, respectively and C^* [M$_s$M^{-1}] is the solute mass fraction of fluid sources (Voss and Provost, 2002). The two terms on the LHS of equation 6 represented the time rate of change of solute mass within the fluid and on the solid, respectively. The first two terms of the RHS of equation 6 represented the advection and diffusion-dispersion of solute within the aquifer, respectively. The fifth term represented sources and sinks of solute. The finite element solution to equations 5 and 6 has been applied to both two- and three-dimensional problems of salt water intrusion (Peterson and Gingerich, 1995; Oki, 2005).

It has long been recognized that the application of Darcian flow models to karst aquifers represents significant simplification of the actual underlying physical processes that occur within these aquifers (Huntoon, 1998 and Scarrow, 1989). The limitations of such an approach was illustrated by Huntoon (1998) when he modified the definition of an aquifer as proposed by Loman and others (1972) to include karst aquifers:

A karst aquifer is an aquifer containing soluble rocks with a permeability structure dominated by interconnected conduits dissolved from the host rock which are organized to facilitate the circulation of fluid in the down gradient direction wherein the permeability structure evolved as a consequence of dissolution by the fluid.

Specifically, the application of computer models developed using equations that represent groundwater flow under Darcian conditions in a continuous homogeneous aquifer to a karst aquifer will underestimate the groundwater flux that occurs through conduits, even when extremely large values of permeability are used in the model equations. Also, as implied in the above quoted definition, this underestimation increases in the down gradient direction as conduit flow increasingly dominates groundwater flux within the karst aquifer.

The problems associated with attempting to apply numeric models to karst aquifers are substantial, and when a sufficient data base of aquifer response characteristics has been created, modeling groundwater flow velocity and direction becomes redundant (Palmer, 1992; Teutach and Sauter, 1992; and Huntoon, 1998). However, constructing a numeric model of a karst aquifer based on sufficient hydrogeologic and climatic data is extremely useful for water resource management purposes. Such a three-dimensional numeric model calibrated to a sufficiently definitive data set could be used successfully to simulate the effects of various production scenarios on aquifer integrity.

Boundary Conditions

For a mathematical model, such as those of equation 3, 4, 5, and 6, to prove useful it is necessary that the model be well posed. In order to call a mathematical model well posed 1) a solution must exist, 2) the solution must be unique, and 3) the solution must depend continuously on the problem data. The problem data are the coefficient, the boundary and initial conditions, and the region on which the model is required to hold. Assuming that all model coefficients have been defined, that the initial distributions of pressure and solute mass are know, and that the solution domain is well defined, the only remaining unknown required to make equations 5 and 6 well-posed are the boundary conditions. There are generally, three types of boundary condition: 1) Dirichlet or specified value, 2) Neumann or specified flux and 3) mixed or radiation boundary conditions.

Depending upon the dimensionality of the problem, one-, two-, or three-dimensional, two, four, or six boundary conditions will be needed, respectively. For a two-dimensional, vertical cross-section, simple carbonate island, model four boundary conditions are needed. The first boundary condition, the top surface, is defined by a time variable specified flux, namely aquifer recharge. The second boundary condition, the ocean edge, is defined by a time variable specified pressure value related to the sea level. The third and fourth boundary conditions, the bottom of the aquifer and water table divide, are a special case of the specified flux boundary condition, the no-flow boundary. These conditions would be similar for the carbonate cover and composite island models, with different physical interpretations of the bottom and landward edge boundary conditions. For a three-dimensional model, no-flow conditions could be applied to the two extra side boundaries, assuming that they are parallel to flow lines. This assumption may result in inaccurate results if internal sources or sinks (i.e. pumping or injection wells) are included in the simulation. This leaves us with two time variable boundary conditions to define for a well-posed model, namely the time-variable aquifer recharge and sea level.

Recharge

   Recharge to the Lens has been defined as the difference between precipitation and evapotranspiration (Mink, 1976). Guam receives approximately 2450 mm yr^{-1} of precipitation on average. Despite the islands small size there maybe as much as a 20% difference in precipitation volume among recording stations on the island during one year (Landers, 1997). Generally, the measurements of precipitation are more accurate and more readily obtained than measurements of evapotranspiration. Several methods have been used to determine the rate of evapotranspiration these include pan evapotranspiration (Mink, 1976), Blandy-Criddle method (CDM, 1982), and a water balance method based upon data obtained for watersheds of Southern Guam (Mink, 1976). These methods of evapotranspiration estimation have resulted in a large range of evapotranspiration rates, reported rates vary from 900 mm yr^{-1} to 2000 mm yr^{-1} (Mink, 1976).

   Another method to estimate exploitable recharge, the amount of recharge that is retained by the Lens long enough to be available for extraction, was developed by Jocson et al. (1999). This method assumes that precipitation falling at a rate of less than 6 mm d^{-1} is returned to the atmosphere via evapotranspiration, precipitation falling at a rate between 6 mm d^{-1} and 50 mm d^{-1} provides exploitable recharge and all precipitation falling at a rate greater than 50 mm d^{-1} is lost to coastal discharge. Using this method Jocson et al. (1999) determined that approximately 60 percent of mean annual precipitation (1470 mm yr^{-1}) arrives at the Lens as exploitable recharge.

   On Guam precipitation volume varies greatly from year to year, due to variability in large-scale atmospheric phenomenon. Within a given year Guam generally experiences a wet season lasting from July to December and a dry season lasting from January to June (Landers, 1997; Lander and Guard, 2003). This seasonality is governed primarily by the seasonal shift of the monsoon trough. During the dry season the monsoon trough is located in the southern hemisphere and easterly trade winds prevail upon Guam (Landers, 1997). During typical years the monsoon trough begins to migrate north during April and May and is usually located over the western north-Pacific (WNP) by July and August. The monsoon trough is associated with deep convective clouds, meso-scale convective cloud systems, and tropical cyclones. Lander (1997) has shown that approximately 12 percent of all precipitation on Guam is related to tropical cyclones that pass within 180 n mi of Guam. Landers (1997) also speculates that a much larger percent of precipitation maybe associated with tropical cyclones; however, these systems may not have fully developed when passing near Guam or may have passed further than 180 n mi from Guam. During 2004 the Joint Typhoon Warning Center (JTWC, 2004) reported 32 tropical cyclones within the WNP, of these 11 passed near or formed in the vicinity (350 km) of Guam (Table 1).

   Global scale atmospheric phenomenon such as El Niño, the intense warming of the eastern equatorial Pacific, significantly affects annual precipitation on Guam (Lander, 1997). El Niño results in an increase in atmospheric pressure over the WNP and a drop in the easterly trade wind intensity (Lander, 1997). These two factors result in reduced precipitation on Guam, during the year flowing an El Niño. Specifically, the end of the wet season may be unusually dry and the following dry season may also be unusually dry (Lander, 1997).

Sea Level

Generally, previous hydrogeologic studies of the Lens have treated sea level as a constant, specified value (Contractor, 1981a; Contractor, 1981b; Contractor et al., 1981; Contractor and Sirvastava, 1990; Contractor and Jensen, 2000; Jocson et al., 2002). This is an acceptable assumption when the time period of interest of the study is large enough that daily astronomical tide fluctuations average to approximately zero and short enough that inter-annual sea level changes are not evident. However, sea level varies at all time scales and to properly assess processes affecting the Lens the fluctuations must be taken into account. Processes affecting sea level over time scales longer than several days are: 1) actual increase in the ocean volume due to thermal expansion and contraction of water and changes in ice-cap and glacier volume (eustatic sea level change), 2) change in the land elevation due to tectonic processes or subsidence (local sea level change), and 3) regional shifts in prevailing winds and current resulting in inter-annual change in sea level elevation. Superimposed upon these longer-term sea level changes are shorter-term changes in sea level caused by the astronomical tides and local weather patterns.

Short-term changes in sea level caused by astronomical tides are easy to predict. These tides result from the orbit of the earth about the sun and the moon about the earth. A series of well established harmonic functions may be used to accurately predict the astronomical tide height once the appropriate harmonic constants have been determined for a given location (Schuremam, 2001). The second factor effecting short-term change in sea level, local weather patterns, is more difficult to predict. Tropical cyclones passing Guam may result in local sea level change depending upon the direction of the prevailing wind and atmospheric pressure. For locations on the west coast of Guam strong westerly winds will tend to increase the tide height, while strong easterly winds will tend to have the opposite effect. El Niño may cause longer-term changes in sea level due to shifts in regional winds and currents. These longer-term sea level changes may have a significant effect upon aquifer processes. During El Niño events the prevailing winds in the WNP are weaker than normal resulting in lower sea levels (Sturman and McGowan, 1999).

MATERIALS AND METHODS

Precipitation volume, water table elevation, and specific-conductance were collected at four deep monitoring wells (EX-6, EX-7, EX-10, and GHURA) within the Yigo-Tumon sub-basin of the Lens (Figure 2) from May 25, 2004 to February 25, 2005. Each of the wells was selected because; in the past the bottom of the well was in or below the freshwater/salt water transition zone (Table 2). One rain gage and one water-level transducer were located at each well. Several specific conductance probes were distributed through the transition zone of each well, the exact location of each probe is shown in Table 2. These devices record data at different frequencies. Hourly data are reported herein. Figure 4 a-d illustrates when the monitoring instruments were out of calibration or were not functioning. At approximately 6 week intervals during the study specific-conductivity profiles were collected at each of the wells. Figure 4 a-d presents the times of each well profile.

Table 1. Tropical cyclones active in the northern west-Pacific during 2004, their name, period of activity, date of closest approach to Guam, and distance of closest approach to Guam (JTWC, 2004)

TC*	Name	Period	Date of Closest Approach	Distance of Closest Approach
				(km)
TS01W	-	11/Feb - 16/Feb	12/Feb	347**
TS02W	-	16/Mar - 22/Mar	15/Mar	918
TY03W	Sudal	04/Apr - 15/Apr	07/Apr	381
STY04W	Nida	13/May - 21/May	13/May	1509
TS05W	-	14/May - 18/May	14/May	3437
TY06W	Omais	16/May - 22/May	16/May	824
TY07W	Conson	04/Jun - 11/Jun	10/Jun	2366
TY08W	Chanthu	07/Jun - 23/Jun	05/Jun	820
STY09W	Dianmu	13/Jun - 21/Jun	15/Jun	841
TY10W	Mindulle	22/Jun - 23/Jun	22/Jun	194**
TY11W	Tingting	25/Jun - 04/Jul	27/Jun	347**
TS12W	Kompasu	13/Jul - 16/Jul	12/Jul	1448
TY13W	Namtheun	25/Jul - 01/Aug	24/Jul	985
TY14W	Meranti	03/Aug - 08/Aug	02/Aug	2329
TD15W	Malou	04/Aug - 05/Aug	02/Aug	1032
TY16W	Rananim	07/Aug - 12/Aug	07/Aug	1607
TS17W	Malakas	10/Aug - 12/Aug	10/Aug	1521
TY18W	Megi	13/Aug - 19/Aug	13/Aug	131**
STY19W	Chaba	18/Aug - 31/Aug	22/Aug	131**
TY20W	Aere	19/Aug - 26/Aug	18/Aug	440
TS21W	-	26/Aug - 28/Aug	28/Aug	274**
STY22W	Songda	27/Aug - 07/Sep	31/Aug	533
TY23W	Sarika	04/Sep - 07/Sep	05/Sep	573
TY24W	Haima	12/Sep -13/Sep	11/Sep	2745
TY25W	Meari	20/Sep - 29/Sep	19/Sep	137**
STY26W	Ma-on	04/Oct - 09/Oct	01/Oct	682
TY27W	Tokage	12/Oct - 20/Oct	12/Oct	99**
TY28W	Nock-ten	12/Oct - 26/Oct	20/Oct	220**
TY29W	Muifa	14/Nov - 26/Nov	13/Nov	1265
TY30W	Nanmadol	28/Nov - 3/Dec	29/Nov	677
TS31W	Talas	10/Dec - 19/Dec	13/Dec	347**
TS32W	Noru	17/Dec - 21/Dec	19/Dec	275**

* Tropical Cyclones: TD –Tropical Depression (≤ 33 kt), TS – Tropical Storm (34 to 63 kt), TY – Typhoon (64 to 149 kt), STY – Super Typhoon (≥ 150 kt)
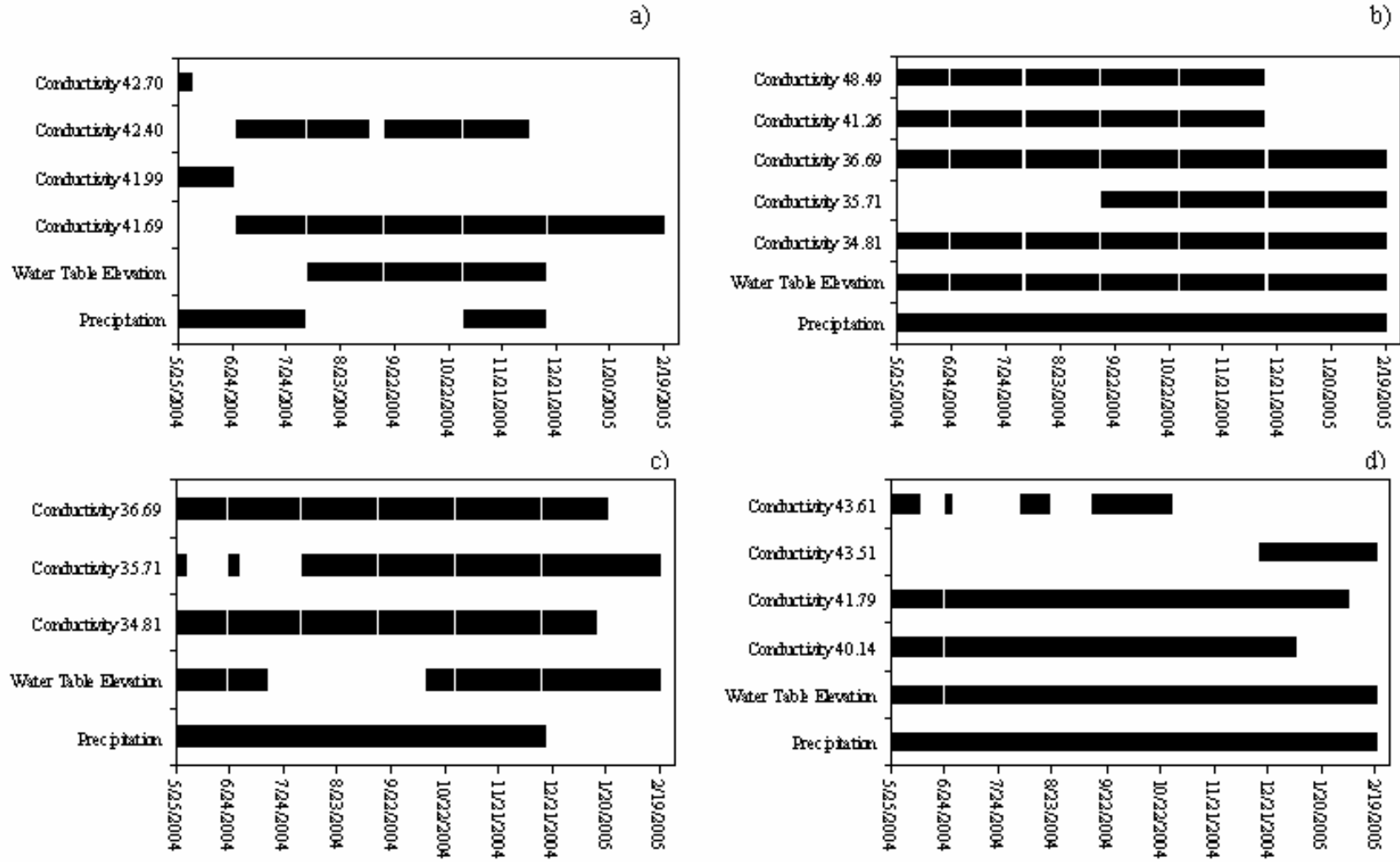** Tropical cyclone closer that 350 km (189 n mi)

Figure 4 a-d. Times when each of the sensors at each of the wells were functioning properly. a) EX-6, b) EX-7, c) EX-10, and d) GHURA-Dededo well

Time Series Data

Rainfall was recorded using tipping bucket rain gages. These gages were located as closely to the wells as possible. At wells EX-6 and GHURA the rain gages were placed 50 and 200 meters for the well, respectively. The rain gages were programmed to record the date and time of each bucket tip. Each tip of the rain gage bucket represents 0.03 cm^3 of precipitation. This data was compiled into hourly precipitation intensity using Microsoft Excel® and Visual Basic®. Figure 4 a-d illustrates the dates when each rain gage was operational.

Table 2. Well specifications including ground surface, water table, transition zone, and bottom of well elevations above mean sea level (amsl). Elevation amsl of conductivity probes. Elevations of the water table and transition zone are based upon data from the beginning of the observational period.

	EX-6	EX-7	EX-10	GHURA
			(m)	
Ground surface	93	86	106	121
Water table	1.28	1.19	1.01	1.24
Beginning transitions zone	-12.91	-10.66	-9.71	-12.23
End transition zone	-12.93	-15.59	-12.86	-14.26
Bottom of well	-44	-127	-109	-237
Conductance 1	-41.98	-34.81	-32.27	-40.14
Conductance 2	-41.99	-35.71	-35.54	-41.79
Conductance 3	-42.40	-36.69	-37.95	-43.51
Conductance 4	-42.70	-41.26		-43.61
Conductance 5		-48.49		

Water table elevation was recorded using either an Odyssey or In-Situ vented water level transducer. Water-level data from the loggers were adjusted to manual measurements taken during the initial installation or on subsequent field visits. Water table values were taken at different intervals ranging from every six minutes to every 15 minutes during the study period. In order to maintain consistency between all measuring devices water-level data were filtered to include only hourly values. Figure 4 a-d outlines the dates when each water level transducers was operational.

Specific-conductance time series were recorded using either a Hydrolab Mini-Sonde or Solinst LTC loggers. These loggers were calibrated prior to initial deployment and at approximately 6-week intervals during the study period. Sampling frequency for the specific-conductance loggers was very erratic. The lowest sampling frequency was 1 h^{-1} therefore; all data were filtered to include only data collected at that frequency. Table 2 shows the location of the specific-conductance loggers within each of the wells. Figure 4 a-d outlines the dates when each specific-conductance logger was operational.

Profile Data

At approximately 6-week intervals specific conductance profiles of each of the 4 monitoring wells were conducted. Profiles were performed using an Ocean Sensor CTD

(conductivity/temperature/pressure sensor). The CTD was lowered into the well using a stainless-steel line and electric deep-sea fishing winch. The dates of the profiles appear as short gaps in the time series data on Figures 4 a-d.

Ocean Level Data

The ocean level was recorded at Agana Boat Basin by the USGS. Data were obtained from the University of Hawaii Sea level Center (http://ilikai.soest.hawaii.edu). Funding for the center was provided by the National Ocean Service of the National Oceanic and Aeronautic Administration with support form the Joint Archive for Sea level which was a cooperative effort between the U. S. National Oceanographic Data Center and the University of Hawaii Sea level Center.

Weather Data

Preliminary climatological data were collected and recorded daily by the National Weather Service at Guam International Airport. These data include daily minimum and maximum temperature, average temperature, daily precipitation, average wind speed, and average wind direction. Preliminary climatology data are available at www.prh.noaa.gov/pr/guam/, data are available from January 2002 to present.

RESULTS AND DISCUSSION

Precipitation

Figure 5 shows the daily precipitation as measured at each of the 4 monitoring locations. During the complete period of record the rain gages at wells EX-7 and GHURA recorded 2.97 and 2.71 m of precipitation, respectively. At wells EX-6 and EX-10 the rain gages recorded 1.42 and 2.71 m of precipitation, respectively. These values compared well with the other gages taken over the same period. During the period when the rain gage at well EX-10 was operational the rain gages at wells EX-7 and GHURA recorded 2.81 and 2.71 m of precipitation, respectively. During the period when the rain gage at well EX-6 was operational EX-7, EX-10, and the GHURA rain gages recorded 1.43, 1.49 and 1.42 m, respectively.

These data illustrate the onset of the wet season during the beginning and middle of June and its premature end during the beginning of October. Ten tropical cyclones passed within 350 km of Guam during the period of record (Table 1). These tropical cyclones provided a significant proportion of the rain that fell during the 2004 wet season. Specifically, 40, 40, and 41 percent of recorded precipitation at wells EX-7, EX-10, and GHURA was associated with tropical cyclones passing near Guam, respectively. Early August 2004 experienced significant rainfall and no tropical cyclone activity. Figure 6 shows that during this period the dominant wind direction was from the northwest. This pattern of significant rainfall and northwest winds indicates that the monsoon trough was near Guam. With the exception of early August and periods when the winds were affected by tropical cyclones the average daily wind direction was from the northeast. These easterly trade winds are associated with reduced rainfall as

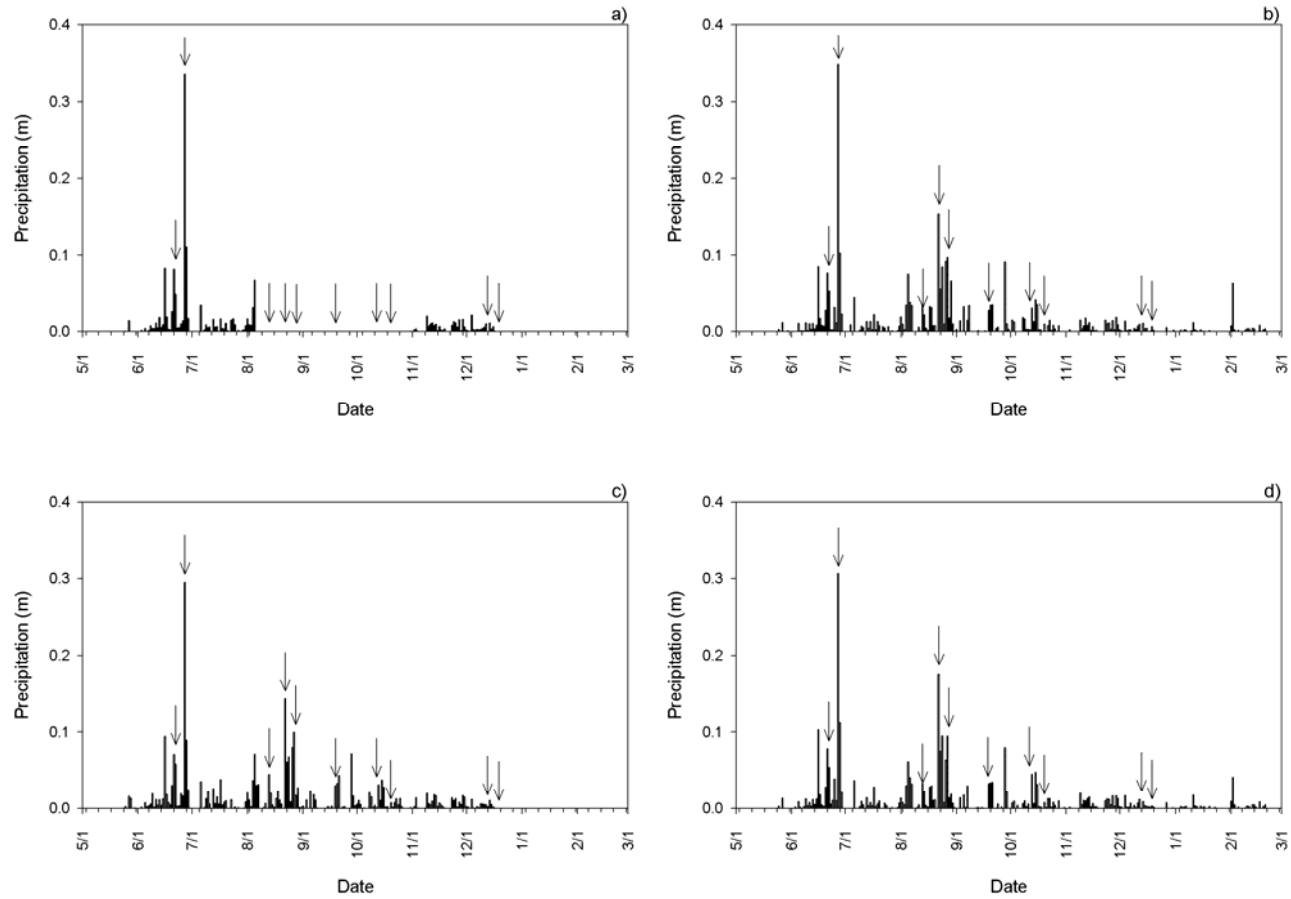Figure 5 a-d. Daily precipitation (m) as measured at each of the four monitoring locations a) EX-6, b) EX-7, c) EX-10, and d) GHURA Dededo. Arrows indicate the passage of a tropical cyclone within 350 km of Guam.
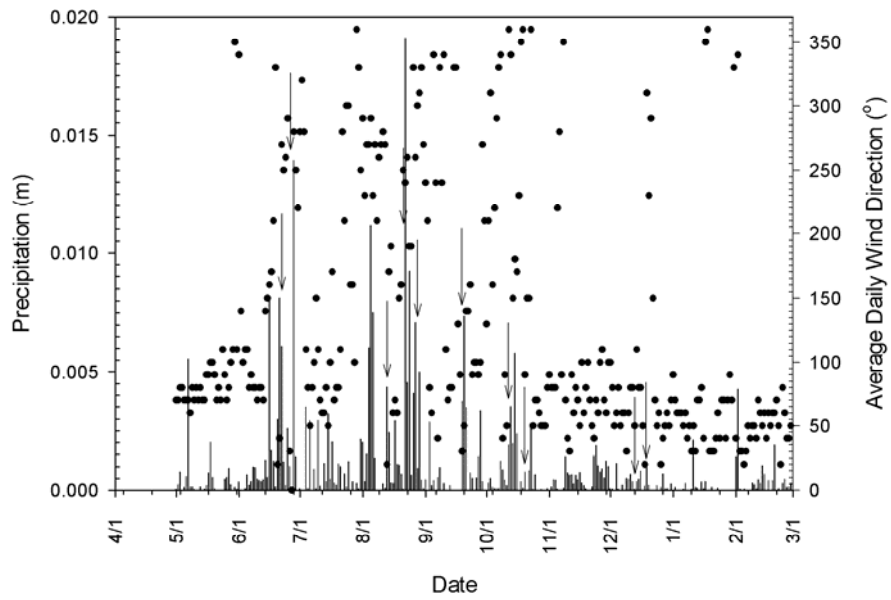
Figure 6. Daily precipitation (bars) and the daily average wind direction (points) as measured by the NWS at Guam International Airport. Arrows indicate the passage of a tropical cyclone with in 350 km of Guam.

illustrated during the end of October, November, and most of December (Figure 5 and 6). These patterns of wind and rainfall are consistent with the weak El Niño event that was experienced during 2004.

Sea Level and Tides

Generally, during the period of record two high and two low tides occur each 24 hour period; this pattern of tides is term as bi-diurnal. Typically, one of the high tides was higher than the other and one of the low tides was lower than the other. These bi-diurnal tides were superimposed upon a 28-day cycle (Figure 7). The bi-diurnal and semi-monthly sea level fluctuations were associated with the orbit of the moon about the earth and the earth about the sun. Although there were a few astronomical tidal forces that have return periods of greater than one month these play only a small role in intra-annual sea level elevation changes. However, large-scale atmospheric phenomena such as El Niño may have a significant impact upon intra-annual sea level in the WNP. During the second half of 2004 and early 2005 there was a gradual downward trend in sea level. The 24-hour averaged ocean level was 1.07 m (amsl) at the end of May, by the beginning of October the 24 hour averaged sea level had dropped to 0.83 m (amsl). The sea level reached its local nadir on January 11, 2005 with a minimum 24 hour average elevation of 0.58 m (amsl). The drop in sea level in the WNP that occurred during the second half of 2004 and early 2005 was associated with a reduction in trade wind strength. This is due to shifting atmospheric circulation patterns associated with El Niño.

The patterns of the astronomic tide are also disrupted by the passage of tropical cyclones. Figure 8a and b shows the effect of four tropical cyclones on sea level. The first, typhoon Tokage, passed approximately 99 km north of Guam on October 12. The winds associated with Tokage were initially from the east (Figure 6) resulting in lower then normal tides (Figure 8a). As typhoon Tokage passed the winds shifted to the west (Figure 6) resulting in higher than normal tides (Figure 8a). The second, typhoon Nock-ten, passed approximately 220 km south of Guam on October 20 (Table 1). The winds associated with the passage of Typhoon Nock-ten were initially westerly then shifting to the east as the storm passed Guam. This resulted in the opposite pattern of tides (Figure 8a) as compared to typhoon Tokage. On December 12 and 19 tropical cyclones Talas and Noru passed Guam, respectively. The winds associated with tropical cyclone Talas were predominately easterly resulting in slightly lower sea levels (Figure 8b). The passage of tropical cyclone Noru resulted in a shift in the wind direction from the east to the west resulting in higher than expected sea levels (Figure 8b). Although the passage of tropical cyclones close to Guam did affect the sea level it was for a relatively short period of time and was a relatively small change in sea level as compared to the effect of El Niño (Figures 7 and 8).
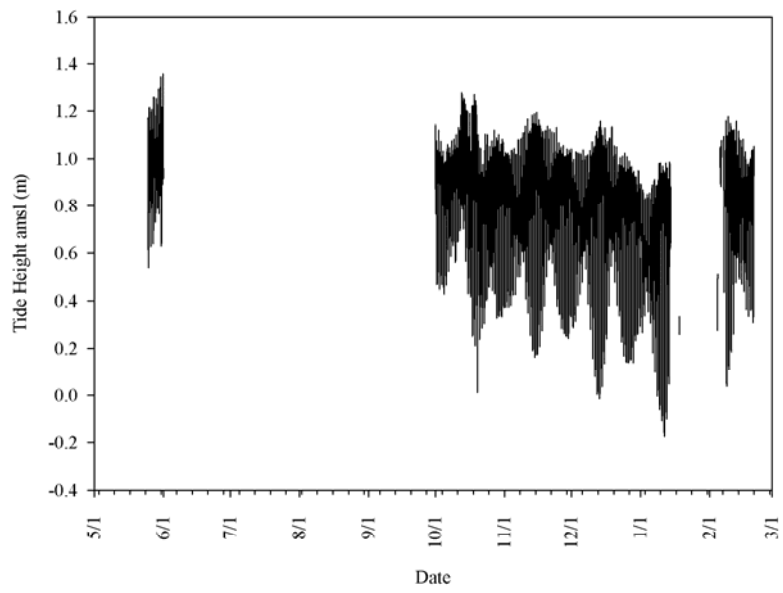
Figure 7. Hourly sea level elevations (m) above mean sea level (amsl) as record at Agana Boat Basin
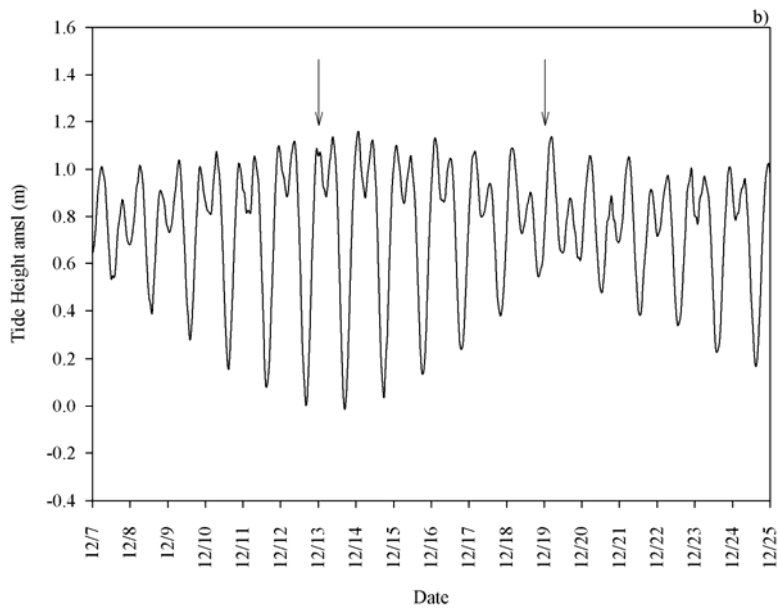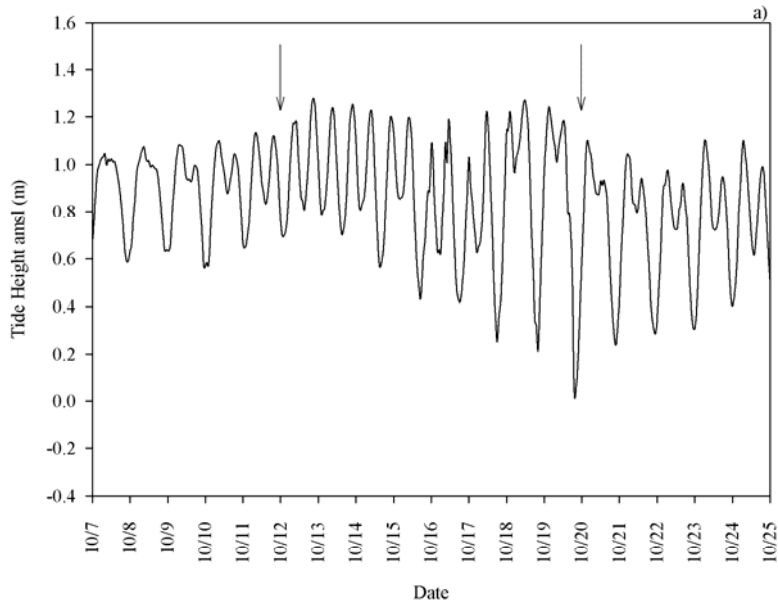
Figure 8a, b. Hourly sea level elevations (m) above mean sea level associated with the passage of typhoons Tokage and Nock-ten (Figure 7a) and Talas and Noru (Figure 7b). Arrows indicate the passage of a tropical cyclone with in 350 km.

Precipitation, and Sea level Effects Upon the Water Table

The pattern of water table elevation fluctuations during the entire study period is illustrated in Figures 9 a-d. Equations 3 and 5 can provide insight into how temporal change in the boundary conditions will affect the water table elevation. These equations show that changes in the water table elevation through time are proportionally related to differences in the potential field through space and the volume of recharge. Depending on the relative value of the terms of the RHS of equations 3 and 5 the water table rises or falls. Variations in the volume of water that recharges the Lens are reflected immediately at observation points within the Lens, according to equations 3 and 5; whereas, changes in water table lag behind sea level change. This lag time is proportional to the distance of the observation point from the coast and the hydraulic conductivity of the aquifer. Additionally, equations 3 and 5 show that changes in the water table elevation due to recharge and sea level change are related to the specific pressure storativity, which for the Lens is approximately equal to porosity. Finally, equations 3 and 5 show that harmonic changes in the sea level are dampened as they propagate through the Lens. This dampening is related to the aquifer properties and the wave length of the sea level fluctuation. These relationships, that are evident in equations 3 and 5, are illustrated by the data (Figure 9 a-d).

Generally, all of the wells experienced a trend of increasing water level from the beginning of June, the start of the rainy season, to the beginning of October. This pattern was followed by a drop in water table elevation beginning in early October continuing to the end of the period of record. This pattern of water table change was related to the relative rates of sea level change and recharge. During the first half of the study period, from May 31, 2004 to October 1, 2004, the average daily precipitation rate (EX-7 19 mm d^{-1}, and GHURA 18 mm d^{-1}) was great enough to result in a rise in the water table elevation (EX-7 0.14 m, and GHURA 0.15 m) while the sea level declined (-0.87 m). However, during the second half of the study period, from October 1, 2004 through January 11, 2005 the average daily precipitation rate (EX-7 6 mm d^{-1}, GHURA 6 mm d^{-1}) was not sufficient to prevent decline in the elevation of the water table (EX-7 -0.17 m, and GHURA -0.14 m) during this period the sea level declined (0.25 m). After the sea level reached its nadir (January 11, 2005) the water table continued to drop at all of the wells. This continued drop in the water table was due to the lack of precipitation during the early winter of 2005.

Large, short-term, increases in water table elevation occur in late June (Figure 9 a-d) and mid to late-August (Figure 10 a-d). These large increases are due to the passage of tropical cyclones. Figure 10 illustrates the effect of very intense rainfall on the water table. The passage of typhoon Tingting resulted in one of the largest one day precipitation events on Guam (EX-6 0.34m, EX-7 0.35m, EX-10 0.30m, and GHURA 0.31m). This large precipitation event resulted in a large perturbation in the water table elevation (EX-7 0.45 m, EX-10 0.36 m, and GHURA 0.35 m). The maximum rate of water table elevation increase lags behind the maximum precipitation rate by between 12 and 18 hrs. This lag represents the mean travel time for water percolating from the ground surface to the water table. The increase in the water table elevation in turn increased the gradient of the potential field resulted in a large discharge rate at the coast. This large discharge rate is evidenced by the rapid rate of water table elevation decline between June 29, 2004 and July 15, 2005 (EX-7 0.03 m d^{-1}, EX-10 0.03 m d^{-1}, and

GHURA 0.03 m d^{-1}). Based upon the foregoing discussion of the effect of tropical cyclones it is reasoned that the passage of typhoon Tingting would have had only a small effect on the sea level and that the vast majority of the water table elevation change is due to an increased rate of recharge.

Figure 11 shows the effect of the passage of typhoons Magi and Chaba and Tropical Storm 21 W on August 13, 22, and 28, 2004, respectively. Although none of these storms had as great a one-day intensity of typhoon Tingting taken as a whole they resulted in more precipitation than Tingting (EX-7 0.73 m, EX-10 0.63, and GHURA 0.69 m). This recharge resulted in a reduced increase in the water table elevation that was sustained for a longer period of time. After the passage of Tropical Storm 21W the water table was once again significantly out of equilibrium with sea level. This period had a similar rate of water table decline (EX-6 0.02 m d^{-1}, EX-7 0.02 m d^{-1}, and GHURA 0.02 m d^{-1}) as compared to period following typhoon Tingting. Smaller increases in the water table are evident in mid-June associated with the passage of typhoon Mindulle and in October associated with the passage of typhoons Tokage and Nock-ten. There was a slight increase in the water elevation beginning in early August that was most likely associated with increased rain due to the proximity of the monsoon trough to Guam (Figure 9 a, b, and d).

Evident in Figures 10 and 11 are bi-diurnal fluctuations of the water table elevation. These fluctuations are related to the bi-diurnal tides experienced at the coast of Guam. The amplitude of the water table fluctuations decreases as the fluctuation prorogates through the aquifer. This amplitude reduction was related to the wave length, aquifer properties and the distance of the observation point from the coast. For the period from May 25, 2004 to June 10, 2004 well EX-10 (0.08 m) had the greatest average daily fluctuation followed by wells EX-7 (0.05 m) and finally GHURA (0.01 m). In Figure 2 it was obvious that well EX-7 was closet to the coast followed by EX-10 and GHURA. Since all of the waves have the same wave length it can be deduced that the aquifer properties must vary throughout the Lens. However, with the current aquifer information that is available there is not a method to determine which aquifer properties vary or how these properties vary spatially.

Precipitation, and Sea level Effects Upon Specific Conductivity

Figures 12 through 15 demonstrate how sea level and recharge affect the specific conductance at several depths within each of the wells. Equation 6 can provide insight into how temporal change in the boundary conditions will affect the specific conductance at any point within the aquifer. The five terms of the RHS of equation 6 can be reduced by making two simplifying assumptions: 1) that there is no production of salt from within the aquifer and 2) that all recharge water contains no salt. By making these assumptions the last three terms of the RHS are equal to zero. Although neither of these two assumptions is strictly true they are adequate for the current level of analysis. Therefore, the time rate of change of specific conductance is related to advection (RHS term 1) and diffusion and dispersion (RHS term 2). Equations 1 and 4 provide some what simplified vision of the interaction of salt water and fresh water. These equations do not account for mixing and equations 1 does not account for the flow of salt water. Because of these assumptions the equations only provide insight into the location of the
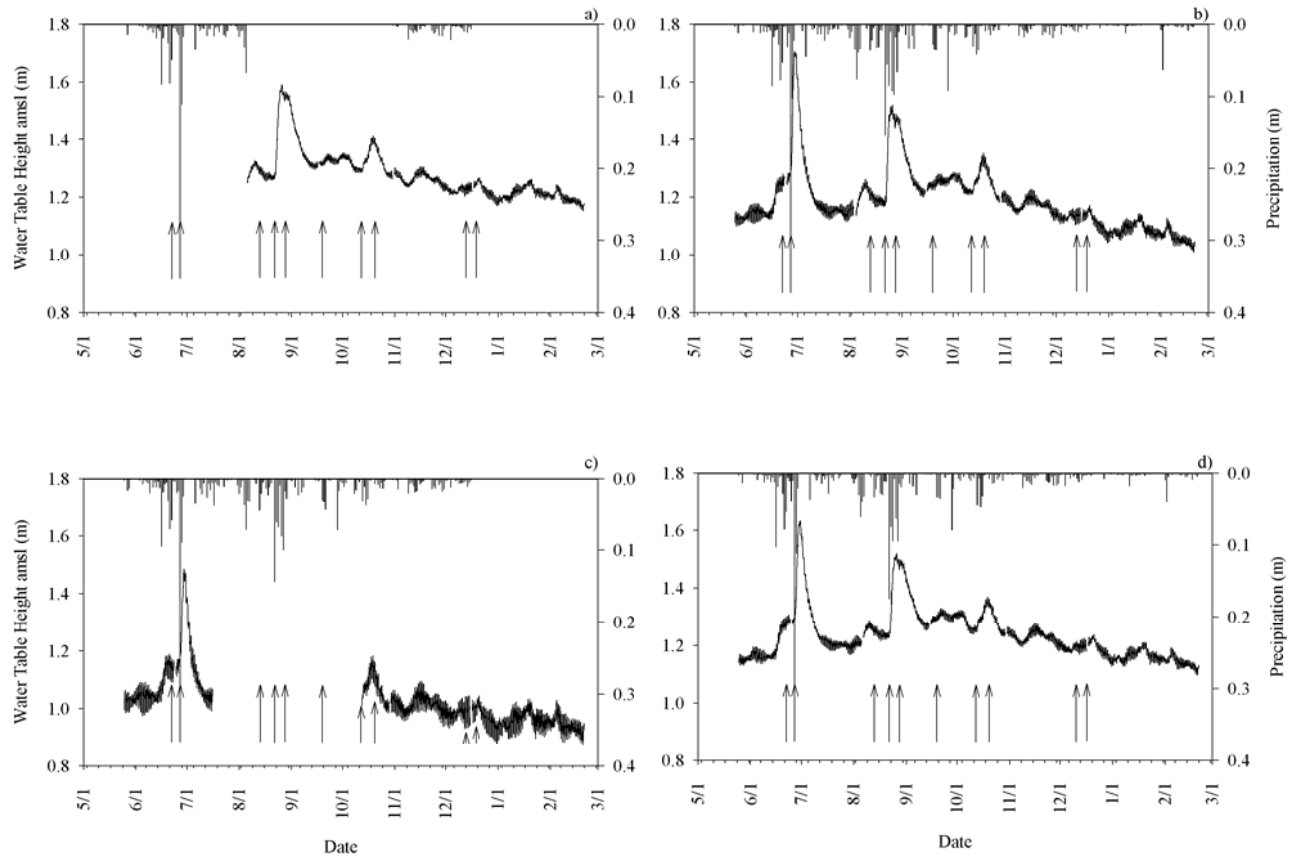
Figure 9 a-d. Water table elevation (m) above mean sea level (amsl) for wells a) EX-6, b) EX-7, c) EX-10, and d) GHURA. Vertical bars are daily precipitation (m). Arrows indicate the passage of a tropical cyclone with in 350 km of Guam.
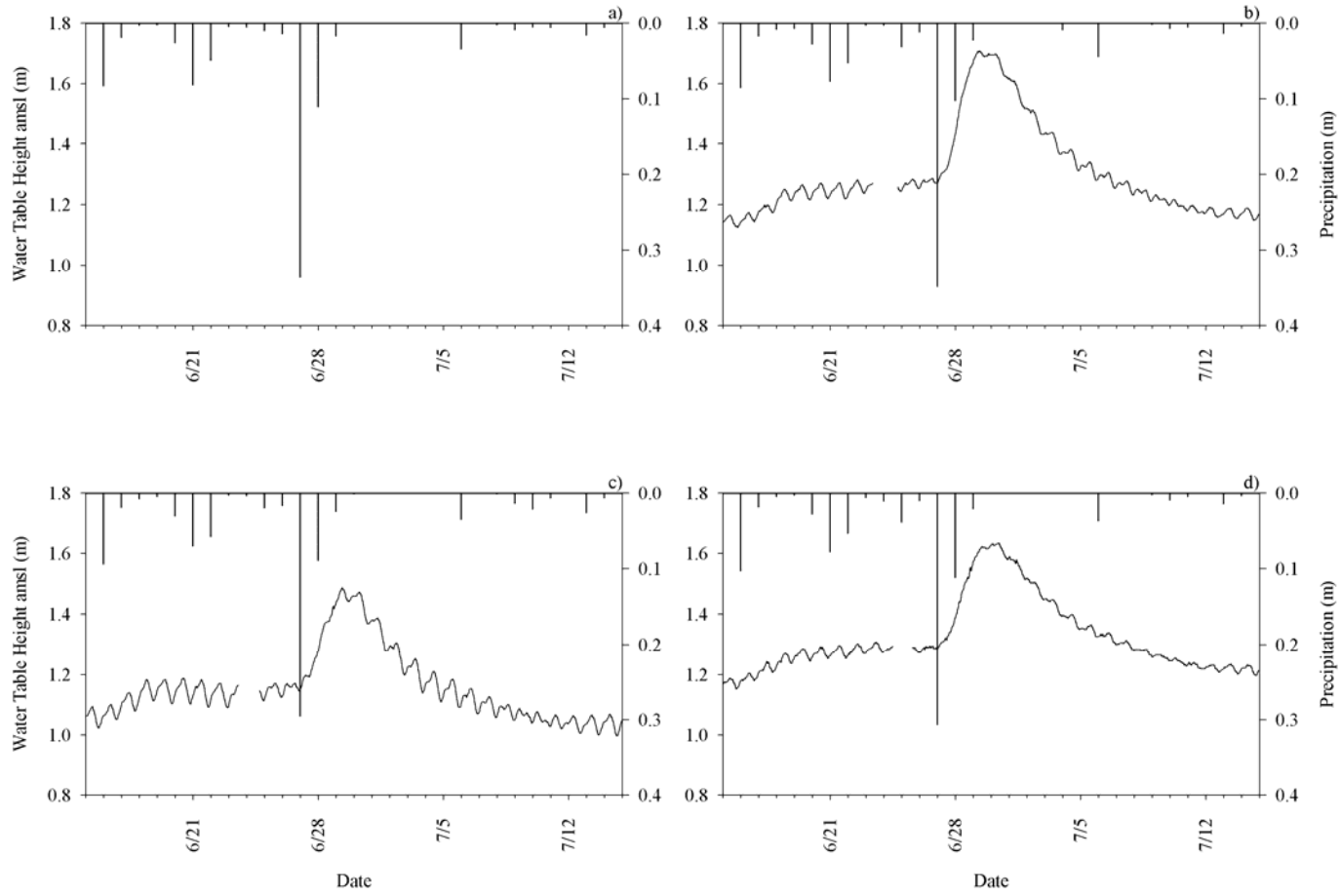
Figure 10 a-d. Water table elevation (m) prior to and following the passage of typhoon Tingting for wells b) EX-7, c) EX-10, and d) GHURA. Vertical bars are daily precipitation (m).
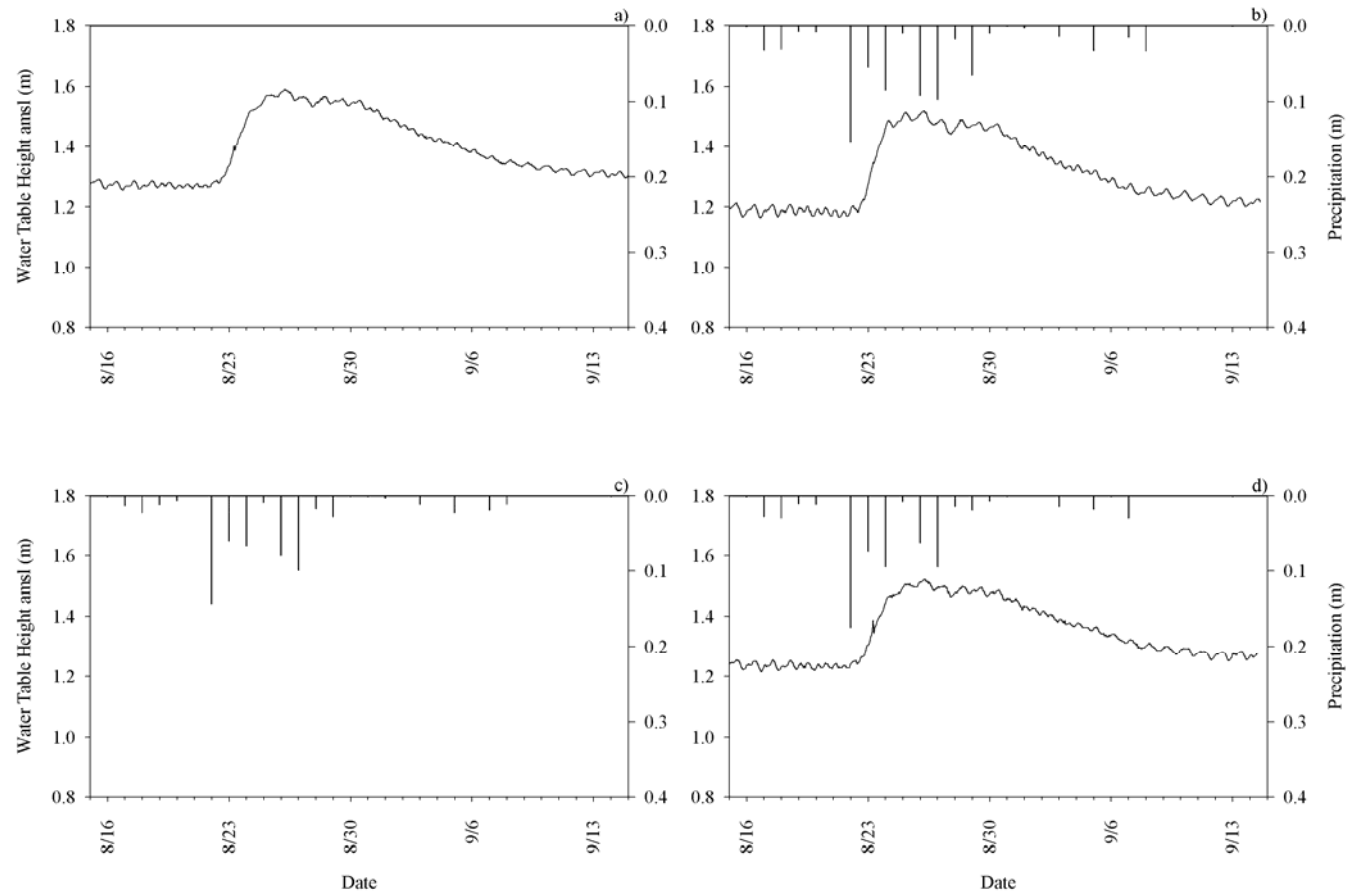
Figure 11a-d. Water table elevation (m) prior to and following the passage of typhoon Megi, super-typhoon Chaba, and tropical storm 21W for wells a) EX-6, b) EX-7, and d) GHURA. Vertical bars are daily precipitation (m).
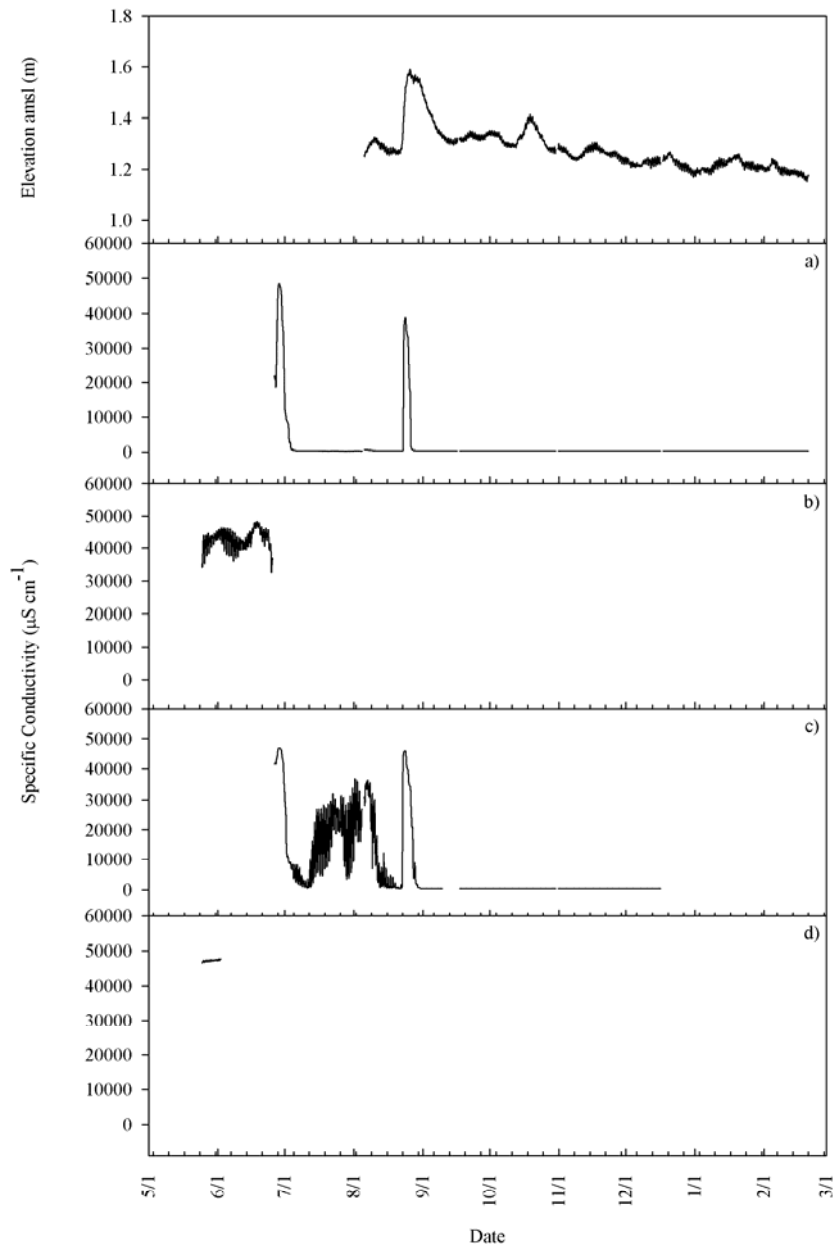
Figure 12. Water table and conductivity time series for well EX-6. Conductivity probes were located at a) -41.98 m (6/26/2004 – 2/20/2005), b) -41.98 m (5/25/2004 – 6/25/2004), c) -42.40 m (6/25/2004 – 2/20/2005) and d) -42.70 m (5/25/2004 – 6/25/2004) (all elevations amsl).
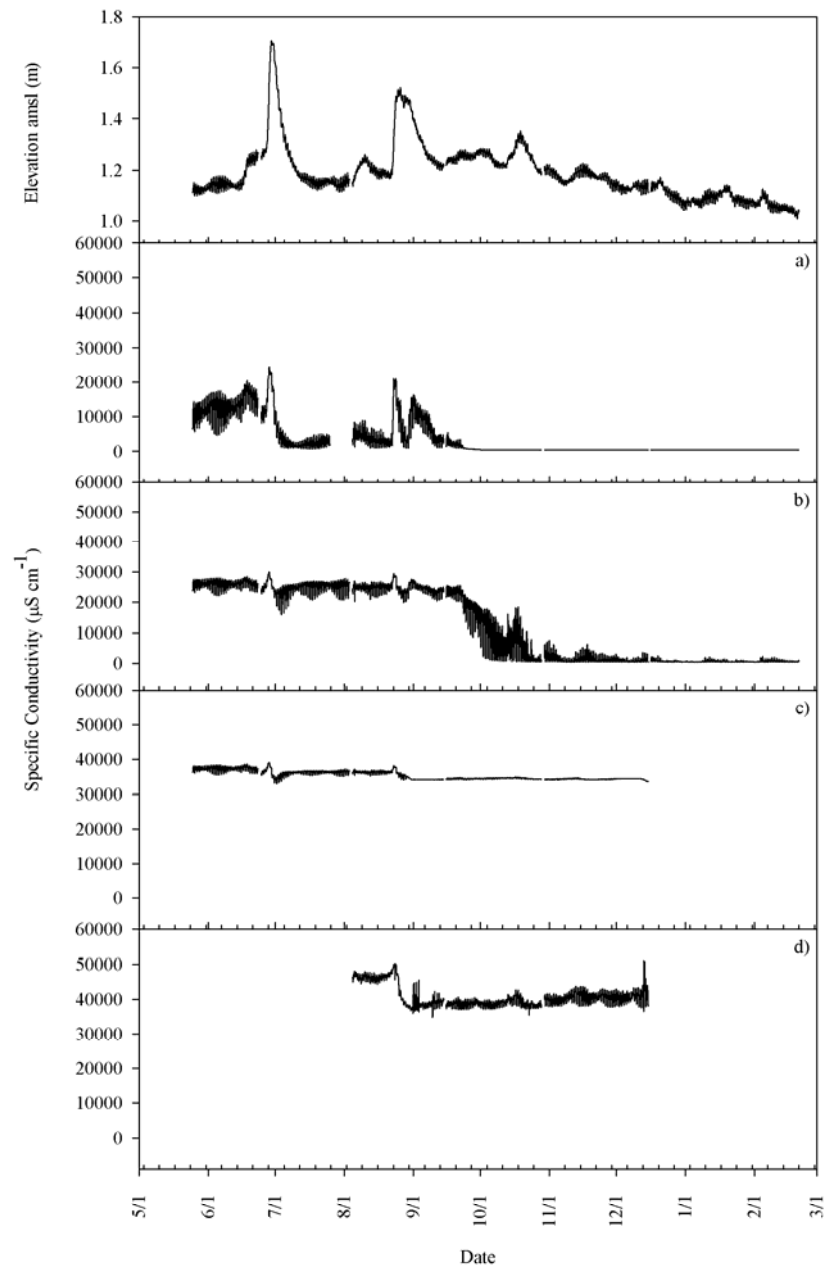
Figure 13. Water table and conductivity time series for well EX-7. Conductivity probes were located at a) -34.81 m (5/25/2004 – 2/20/2005), b) -36.69 m (5/25/2004 – 2/20/2005), c) -41.26 m (5/25/2004 – 12/15/2004), and d) -48.49 m (8/4/2004 – 12/15/2004) (all elevations amsl).
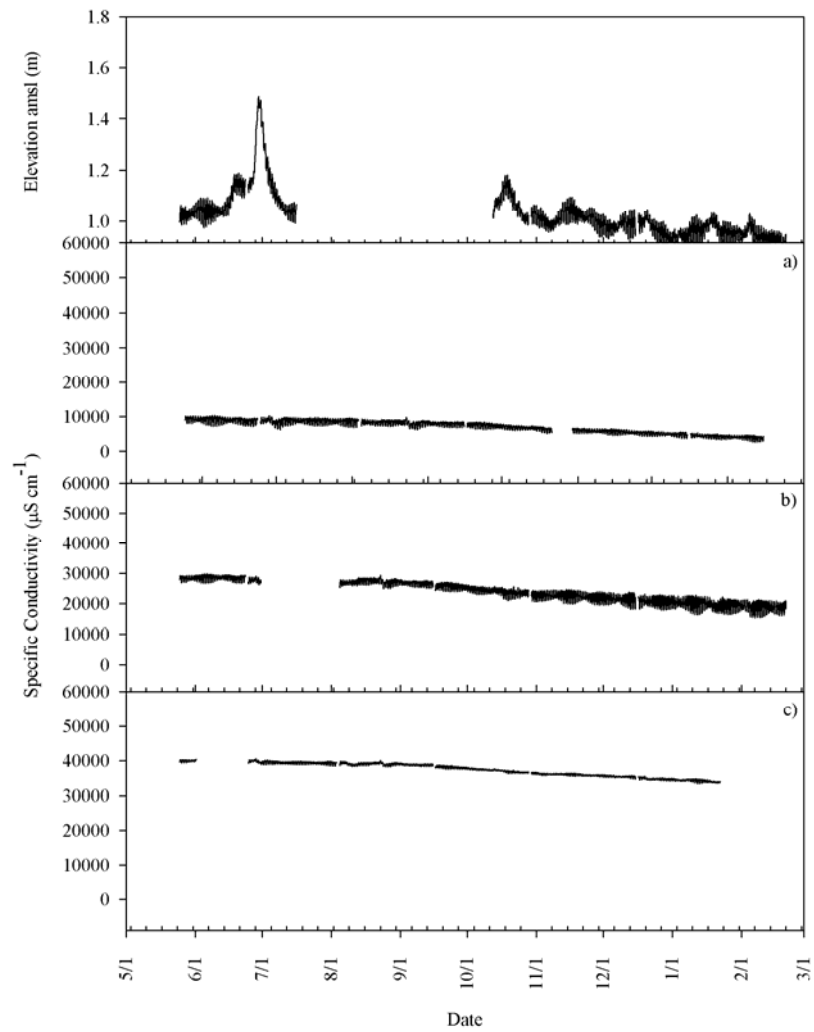
Figure 14. Water table and conductivity time series for well EX-10. Conductivity probes were located at -32.27 m (5/25/2004 – 2/20/2005), -35.54 m (5/25/2004 – 2/20/2005), and -37.95 m (5/25/2004 – 1/22/2005) (all elevation amsl).

Figure 15. Water table and conductivity time series for the GHURA Dededo well. Conductivity probes were located at a) -40.14 m (5/25/2004 – 1/6/2005), b) -41.79 m (5/25/2004 – 2/5/2005), c) -43.51 m (12/17/2004 – 2/20/2005) and d) -43.61m (5/25/2004 – 10/29/2005) (all elevations amsl).
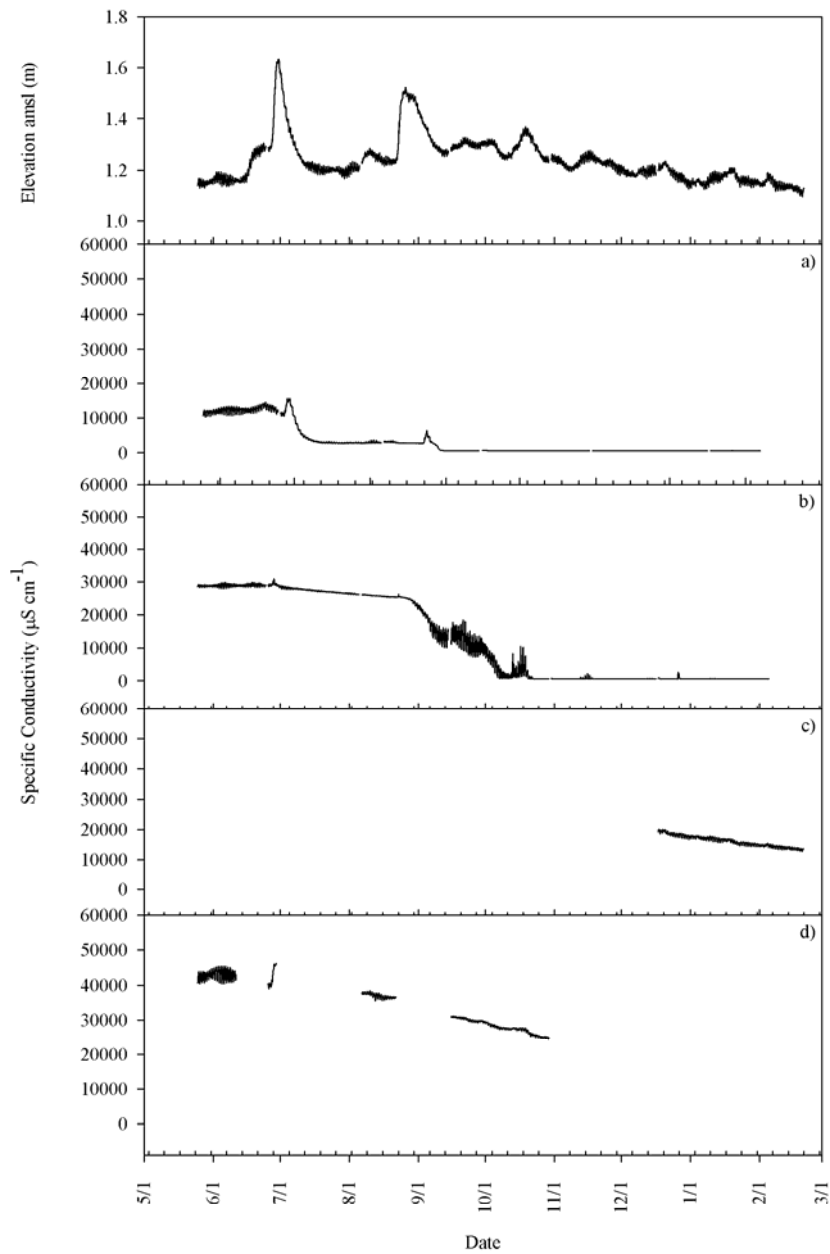
interface center, the fiftieth percentile isochlor. Even though equations 1, 2, and 5 provide a more simplistic view of the salt – fresh water interface, as compared to equation 6, they still provide some insight into lens processes.

It is evident from Figures 12 through 15 that there was a bi-diurnal fluctuation of specific conductance at all four monitoring locations; as with the water table this fluctuation is related to the bi-diurnal tide at the coast of Guam. The bi-diurnal fluctuation in specific conductance is in-phase with the water table. That is, as the elevation of the water table increased the value of specific conductance at a specific spot within the aquifer increased. This increase in specific conductance was due to the propagation of the tide signal through the entire aquifer, not just at the water table surface. This signal was a wave, a harmonic fluctuation in potential energy. As this energy wave moved through the aquifer, water flowed toward the lower energy, the wave trough, and away from the higher energy, the wave peak. This results in an overall elliptical motion of water and salt molecules within the aquifer. The relative magnitude of the bi-diurnal specific conductance fluctuations vary from well to well within the aquifer and from probe to probe within wells. These changes in specific conductance are related to 1) the damping of the tidal motion due to aquifer properties and 2) the vertical rate of change of specific conductance at a well. Specifically, in a well with a sharp transitions zone (i.e. EX-6) there is a large bi-diurnal fluctuation in specific conductance (Figure 12 c), in wells with a more gradual transition zone (i.e. EX-10) there was a reduced bi-diurnal fluctuation (Figure 14 a-c). The bi-diurnal fluctuation of the entire aquifer contributes to the formation of the transition zone. However, this is not the only factor influencing the formation of the transition zone. This is evidenced by comparing well EX-6 and EX-7 that have similar bi-diurnal water table fluctuations but very different transition zones.

The passage of tropical cyclones affected the distribution of specific conductance within the aquifer. However, unlike the effect on the water table, where all water table elevations increased proportionally to the volume of rainfall, changes in specific conductivity varied from well to well. Wells EX-7 and GHURA showed similar patterns of specific conductance response to the passage of typhoons. Generally, the shallowest probe experienced a sharp drop in specific conductance after the passage of typhoon Tingting. Deeper probes showed very little response to the passage of Tingting. However, after the tropical cyclones of mid and late August the next shallowest probes experienced a sharp specific conductance drop. During the entire period of record the deepest probes never experienced sharp drops in specific conductance related to typhoons. At well EX-10 there was only a very slight effect of tropical cyclones upon specific conductance values. Finally, EX-6 showed widely fluctuating values of specific conductance during the passage of typhoon Tingting and Magi. Specifically, the value of specific conductance spikes during the storm and falls off very rapidly following the storm. These spikes in specific conductance are evident at each of the other wells. The spikes are most prominent at well EX-6 due to the sharp salt – fresh water interface. These spikes may be due to enhanced mixing due to increased water flow velocity within the aquifer.

Deeper probes at the GHURA well and all of the probes at well EX-10 showed a gradual decline in specific conductance through out the period of record. The deeper probes at well EX-7 remained approximately constant through time. Neither of these

patterns was consistent with the models proposed by equations 1 and 2, where the interface should rise with a drop in water table elevation. These models, however, do not account for the drop in sea level that was experienced during the period of record. The drop in sea level may account for the long term trends that are evident in the data. Another possible explanation for the long term drop in the position of the interface is a lag between water table processes and interface processes. Change in the water table elevation may occur very rapidly in response to large precipitation events. Whereas, the interface may respond at a much slower rate which may dampen out the effect of individual storms (Figure 14).

Specific Conductivity Profiles

Figures 16 through 19 show the results of the conductivity profiles that were preformed periodically through out the period of record. These profiles are snap shots in time of the conditions of the salt – fresh water interface. With the exception of well EX-6, there is a gradual transition from low specific conductivity, associated with fresh water, to high specific conductance, associated with salt water. The transition zone was widest at well EX-7 were the distance between the 10th and 90th percentile vary from approximately 10 m to more than 20 m. For both the GHURA well and well EX-10 the transition zone was between 5 m and 10 m wide. The width of the transition zone is controlled by the magnitude of the tidal fluctuation as well as by the dispersion and diffusion. Because the diffusion coefficient value for Chloride in water is several orders of magnitude less than the dispersion coefficient value it was assumed that dispersion was the dominant process occurring with in the aquifer.

Assuming that the flow field within the aquifer is homogenous and that there is little material heterogeneity within the lens, there should be a smooth transition between fresh water and salt water. The transition should be balanced around the fiftieth percentile, with the tenth and ninetieth percentiles being the same distance above and below the fiftieth percentile, respectively. This ideal case occurred within well EX-10 through out the year and at the GHURA well during the first half of the period of record. During much of the second half of the period of record the GHURA had a skewed distribution of salt water and fresh water. There was a very rapid transition to the twenty-fifth percentile and then a more gradual transformation for the rest of the transition zone. This skewed pattern occurred at well EX-7 for the entire period of record. These asymmetric distributions may be related to heterogeneous flow fields or heterogeneous or anisotropic aquifer dispersion properties.

CONCLUSIONS

The results of the study reported here clearly show that temporal variability in the boundary condition of the Lens affect the distribution of both fresh water and salt water. Specifically, the effect of the annual rainfall variability upon the lens was demonstrated. During the wettest portion of the wet season the water table rose in response to the excess precipitation. During the Fall of 2004 drier conditions prevailed and the water table fell in response to the combined effects of reduced precipitation and falling sea level. Additionally, the effect of large, short-term storm events was observed. These intense events result in a rapid rise in the water table followed shortly by a rapid fall, if no other precipitation event occurs. The effect of sea level change was also observed during the

Figure 16. Specific Conductance profiles at well EX-6. Dates of specific profiles are indicated above the graph for that profile. The solid horizontal line represents the fiftieth percentile of specific conductance, the dashed horizontal line represent the twenty-fifth and seventy-fifth percentiles, and the dotted line represents the tenth and ninetieth percentiles.
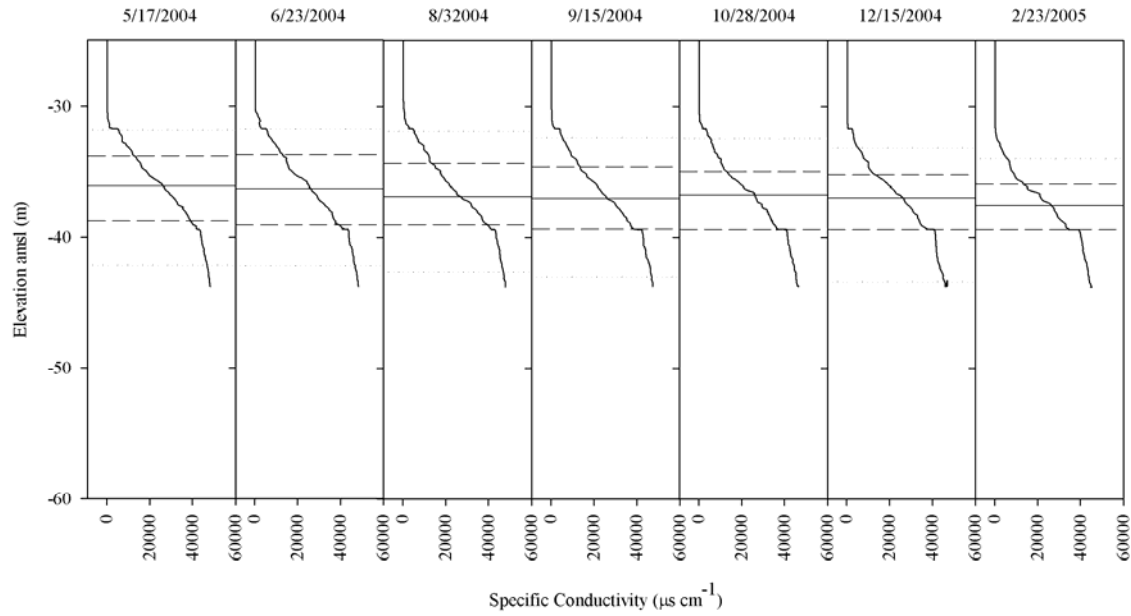
Figure 17. Specific Conductance profiles at well EX-7. Dates of specific profiles are indicated above the graph for that profile. The solid horizontal line represents the fiftieth percentile of specific conductance, the dashed horizontal line represent the twenty-fifth and seventy-fifth percentiles, and the dotted line represents the tenth and ninetieth percentiles.
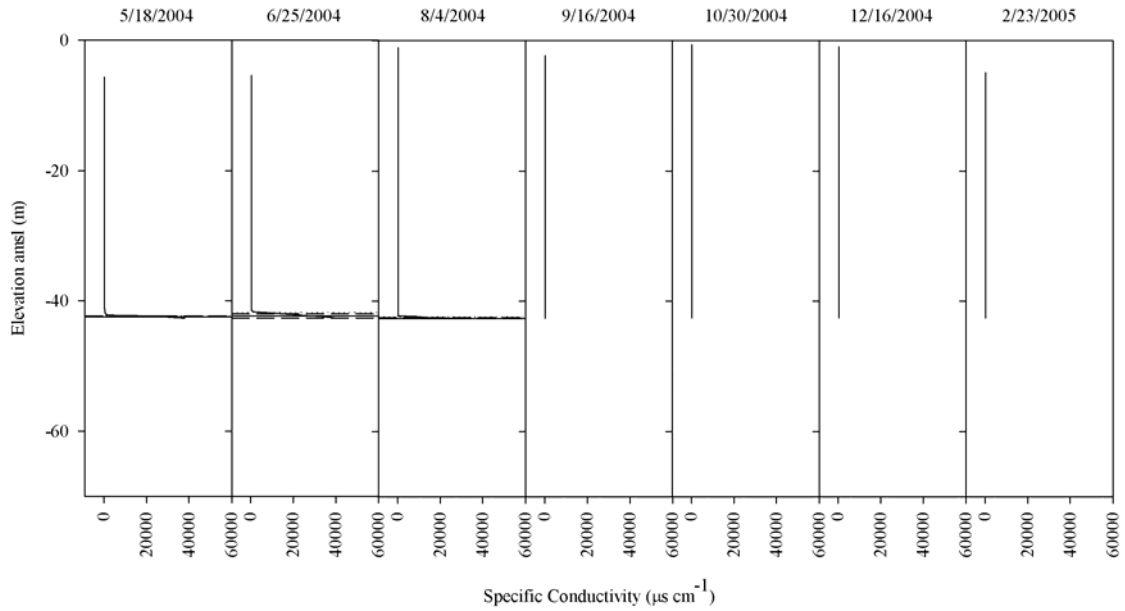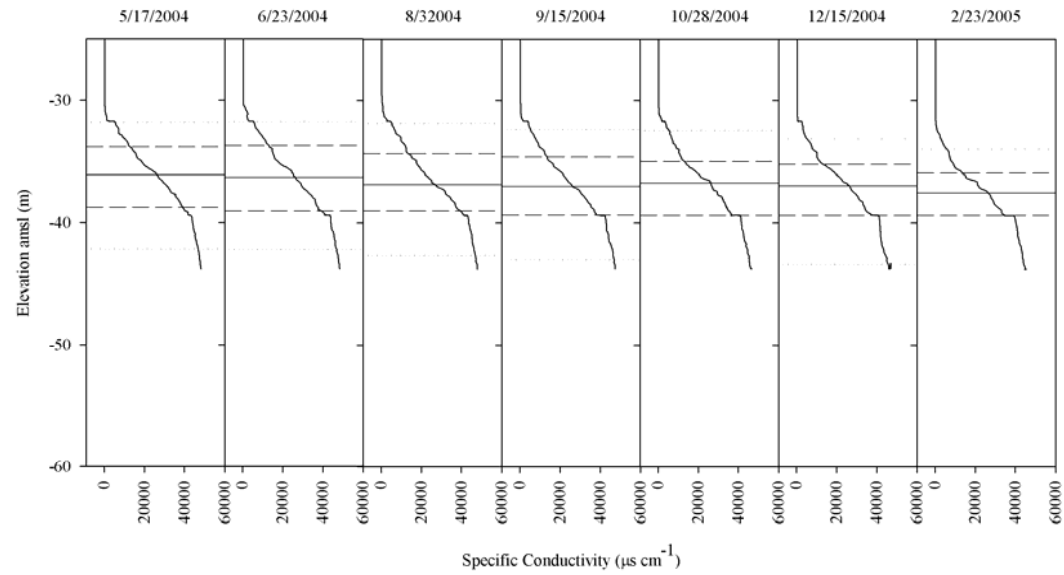
Figure 18. Specific Conductance profiles at well EX-10. Dates of specific profiles are indicated above the graph for that profile. The solid horizontal line represents the fiftieth percentile of specific conductance, the dashed horizontal line represent the twenty-fifth and seventy-fifth percentiles, and the dotted line represents the tenth and ninetieth percentiles..

Figure 19. Specific Conductance profiles at GHURA Dededo well. Dates of specific profiles are indicated above the graph for that profile. The solid horizontal line represents the fiftieth percentile of specific conductance, the dashed horizontal line represent the twenty-fifth and seventy-fifth percentiles, and the dotted line represents the tenth and ninetieth percentiles.
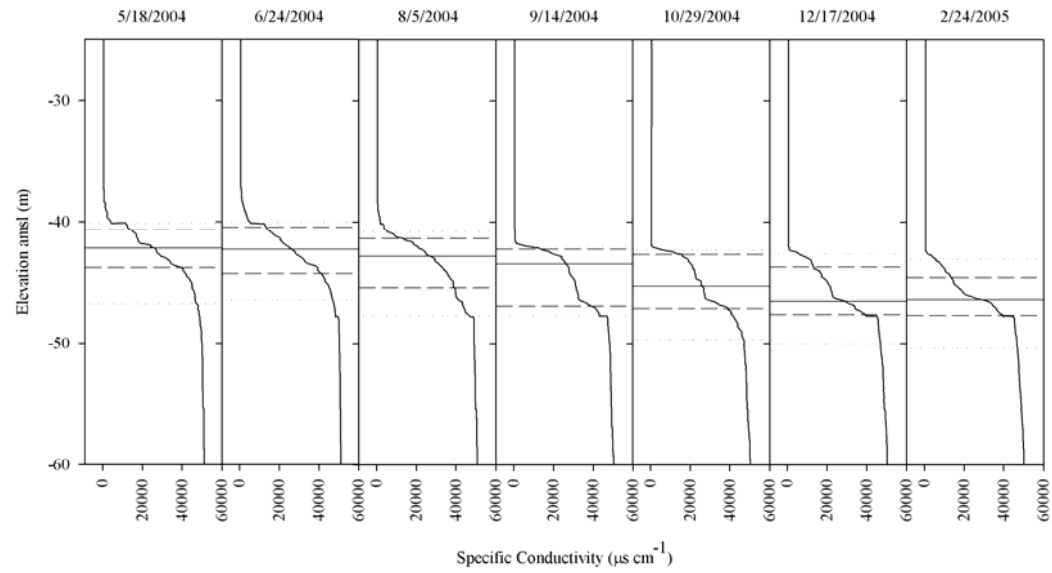
period of record. For the majority of the study period the sea level was falling. During the fall of 2004 this combined with the reduced precipitation resulted in a drop in the water table. The effect of storm surge that is associated with the passage of tropical cyclones was not observed at any well. The precipitation and sea level data observed during this study are consistent with a weak El Niño event.

These same boundary conditions also had a significant impact on the location of the salt – fresh water interface and the shape of the interface at some wells. To the greatest extent the salt – fresh water interface was depressed during the study period. This was the result of the combined affects of a water table elevation fluctuation and sea level elevation decline. Large, short-term storm events tend to influence the upper portion of the interface. Longer-term changes in the water table and sea level elevation influence the entire salt – fresh water interface.

The results of this investigation confirm some of the previous hypothesis concerning lens processes. However, it also raises several new questions that must be addressed to properly manage the lens. Time series analysis methods must be developed that will determine the lag between precipitation and lens recharge. These techniques should also be used to determine the lag time between precipitation events and sea level changes, and changes in the interface. Also, these techniques should be used to determine the lag time between water table elevation changes and interface changes. Coupled with this analysis should be continued development of numerical models that simulate observed Lens geometric dynamics as a function of climatic and boundary variations. The physical processes that influence the water table and the shape and location of the interface could be refined and expanded geographically and temporally by additional monitoring programs such as described herein. Once these studies have been conducted, calculations and simulations should be preformed to refine estimates of sustainable yield.

REFERENCES

Ayers, J. F. and R. N. Clayshulte. 1984. A preliminary study of the hydrology of northern Guam. Technical Report No. 56. Water and Environmental Research Institute of the Western Pacific, University of Guam, Mangilao.

BCG (Barrett Consulting Group). 1992. Groundwater in northern Guam, sustainable yield and groundwater development. Prepared for the Public Utility Agency of Guam. CDM (Camp, Dresser & McKee, Inc.) 1982: Final Report, Northern Guam Lens Study, Groundwater Management Program, Aquifer Yield Report. Prepared for the Guam Environmental Protection Agency.

Contractor, D. N. 1981a. A one dimensional, finite element salt water intrusion model. Technical Report No. 20. Water and Environmental Research Institute of the Western Pacific, University of Guam, Mangilao.

Contractor, D. N. 1981b. A two dimensional, finite element model of salt water intrusion in groundwater systems. Technical Report No. 26. Water and Environmental Research Institute of the Western Pacific, University of Guam, Mangilao.

Contractor, D. N., J. F. Ayers, and S. J. Winter. 1981. Numerical modeling of salt water intrusion in the Northern Guam Lens. Technical Report No. 27. Water and Environmental Research Institute of the Western Pacific, University of Guam, Mangilao.

Contractor, D. N., and J. W. Jenson. 2000. Simulated effect of vadose infiltration on water levels in the Northern Guam Lens Aquifer. Journal of Hydrology. 229: 232-254.

Contractor, D. N., and R. Srivastava. 1990. Simulation of saltwater intrusion in the Northern Guam Lens using a microcomputer. Journal of Hydrology, 118: 87-106.

Cooper, H. H. 1964. A hypothesis concerning the dynamic balance of fresh water and salt water in a coastal aquifer. Geological Survey Water-Supply Paper 1613-C. U. S. Geological Survey. Washington D. C.

Glover, R. E. 1964. The pattern of fresh-water flow in a costal aquifer. Geological Survey Water-Supply Paper 1613-C. U. S. Geological Survey. Washington D. C.

Henry, H. R. 1964. Interfaces between salt water and fresh water in costal aquifers. Geological Survey Water-Supply Paper 1613-C. U. S. Geological Survey. Washington D. C.

Huntoon, P.W. 1995. Is it appropriate to apply porous media ground water circulation models to karstic aquifers? In: Groundwater models for resources analysis and management. Ed. A. El-Kadi. CRC Press. Boca Raton, FL.

Jocson, J.M.U., J. W. Jenson, and D. N. Contractor. 2002, Recharge and aquifer response: Northern Guam Lens Aquifer, Guam, Mariana Islands. Journal of Hydrology. 260: 231-254.

JTWC (Joint Typhoon Warning Center). 2004. 2004 Annual Tropical Cyclone Report. U.S. Naval Pacific Meteorology and Oceanography Center/ Joint Typhoon Warning Center. Pearl Harbor, Hawaii

Keel, T. M., J. E. Mylroie, and J. W. Jenson. 2005. The caves and karst of Rota island, Commonwealth of the Northern Mariana Island. Technical Report No. 107. Water and Environmental Research Institute of the Western Pacific, University of Guam, Mangilao.

Lander, M.A. 1997. Meteorological factors associated with drought on Guam. Technical Report No. 75. Water and Environmental Research Institute of the Western Pacific, University of Guam, Mangilao.

Lander, M. A., and C. P. Guard. 2003. Creation of a 50 year rainfall database, annual rainfall climatology, and annual rainfall distribution map for Guam. Technical Report No. 102. Water and Environmental Research Institute of the Western Pacific, University of Guam, Mangilao.

Lohman, S.W., R.R. Bennett, R.H. Brown, H.H. Cooper, Jr., W.J. Drescher, J.G. Ferris, A.I. Johnson, C.L. McGuinness, A.M. Piper, M.I. Rorabaugh, R.W. Stallman, and C.V. Theis. 1972. Definitions of groundwater terms, revisions and conceptual refinements. Geological Survey Water Supply Paper 1988. U. S. Geological Survey, Washington D. C.

McDonald, M.Q., and J. W. Jenson. 2003. Chloride history and trends of water production well in the Northern Guam Lens aquifer. Technical Report No. 98. Water and Environmental Research Institute of the Western Pacific, University of Guam, Mangilao.

Mink, J. F. 1976. Groundwater resources on Guam: Occurrence and development. Technical Report No. 1. Water and Environmental Research Institute of the Western Pacific, University of Guam, Mangilao.

Mink, J. F. and H. L. Vacher. 1997. Hydrogeology of northern Guam. In: Geology and hydrogeology of carbonate islands. In:Developments in Sedimentology 54. Eds. H.L. Vacher and T. Quinn. Elsevier Science. Amsterdam.

Mylroie, J. E., J. W. Jenson, D. Taborosi, J.M.U. Jocson, D. T. Vann and C. Wexel. 2001. Karst Features of Guam in terms of a general model of carbonate island karst. Journal of Cave and Karst Studies. 63(1): 9-22.

Mylroie, J. E., J. W. Jenson, J. M. U. Jocson, and M. A. Lander. 1999. Karst geology and hydrology of Guam: A preliminary report. Technical Report No. 89. Water and Environmental Research Institute of the Western Pacific, University of Guam, Mangilao.

Oki. D. S. 2005. Numerical simulation of the effects of low-permeability valley-fill barriers and the redistribution of ground-water withdrawals in the Pearl Harbor area, Oahu, Hawaii. Scientific Investigations Report 2005-5253. U.S. Geological Survey, Reston, Virginia.

Palmer. A.N. 1992. Opportunities and pitfalls in the computer modeling of karst aquifers: Ed. A. E. Ogden, Abstracts of the 1992 Friends of Karst, Tennessee Technological University. 20-21.

Peterson, F.L. and S. B. Gingerich. 1995. Modeling atoll groundwater systems. In: Groundwater models for resources analysis and management. Ed. A. I. El-Kadi. CRC Press. Boca Raton, Florida

Scarrow, J.W., 1989. The use of models in groundwater contamination cases. Virginia Environmental Law Journal. 9:185-205.

Schureman, P. 2001. Manual of harmonic analysis and prediction of tides. Special
    Publication No. 98 U.S. Department of Commerce. Washington D.C.

Sturman, A. P. and H. A. McGowan. 1999. Climate. In: The pacific islands
    environment and society. Ed. M Rapaport. The Bess Press, Inc. Honolulu,
    Hawai'i

Teutsch, G. and M. Sauter. 1992. Groundwater modeling in karst terranes, scale effects,
    data acquisition and field validation: Proceedings of the Third Conference on
    Hydrology, Ecology, Monitoring, and Management of Groundwater in Karst
    Terranes (Nashville, TN, December 4-6, 1991), U.S. Environmental Protection
    Agency and National Ground Water Association, p. 17-34

Voss, C. I. and A. M. Provost. 2002. SUTRA: A model for saturated-unsaturated,
    variable-density Ground-water flow with solute or energy transport. Water-
    Resources Investigations Report 02-4231. U.S. Geological Survey. Reston,
    Virginia.

Ward, P. E., S. H. Hoffard, and D. A. Davis. 1965. Hydrology of Guam: Geology and
    hydrology of Guam, Mariana Islands. Vol. 403-H. U. S. Geological Survey
    Professional Paper, U. S. Government Printing Office, Washington D. C.